Systematic Evaluation of Genetic and Environmental Factors Affecting Performance of Translational Riboswitches

R. Kent and N. Dixon*

Manchester Institute of Biotechnology, School of Chemistry, University of Manchester, Manchester M13 9PL, United Kingdom

S *Supporting Information*

ABSTRACT: Since their discovery, riboswitches have been attractive tools for the user-controlled regulation of gene expression in bacterial systems. Riboswitches facilitate small molecule mediated fine-tuning of protein expression, making these tools of great use to the synthetic biology community. However, the use of riboswitches is often restricted due to context dependent performance and limited dynamic range. Here, we report the drastic improvement of a previously developed orthogonal riboswitch achieved through *in vivo* functional selection and optimization of flanking coding and noncoding sequences. The behavior of the derived riboswitches was mapped under a wide array of growth and induction conditions, using a structured Design of Experiments approach. This approach successfully improved the maximal protein expression levels 8.2-fold relative to the original riboswitches, and the dynamic range was improved to afford riboswitch dependent control of 80-fold. The optimized orthogonal riboswitch was then integrated downstream of four endogenous stress promoters, responsive to phosphate starvation, hyperosmotic stress, redox stress, and carbon starvation. These responsive stress promoter−riboswitch devices were demonstrated to allow for tuning of protein expression up to ∼650-fold in response to both environmental and cellular stress responses and riboswitch dependent attenuation. We envisage that these riboswitch stress responsive devices will be useful tools for the construction of advanced genetic circuits, bioprocessing, and protein expression.

KEYWORDS: riboswitch, Design of Experiments, robustness, FACS, synthetic biology, cellular stress
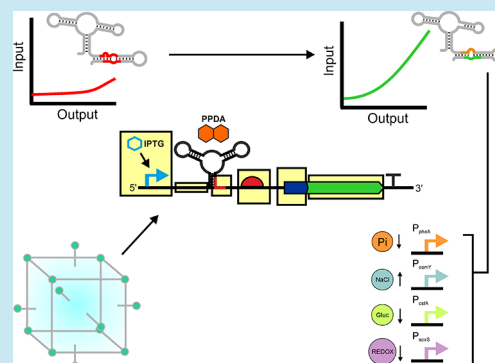
As the desire to construct ever more complex synthetic gene circuits grows, the robust performance of requisite parts becomes ever more important. Genetic circuits often exploit transcription factors to encode logic function.[1−3] The expression of such regulatory proteins can place a significant metabolic burden upon the host cell due to the cost of translation and ribosome sequestration with up to 50% of cellular energetic resources allocated to translation.[4,5] Minimizing the cost of genetic circuitry is a major challenge to the expansion of synthetic biology.[6]

The use of "ribo-regulation" has become a promising alternative to traditional transcription-factor-based systems for heterologous gene expression control. These systems include ribozymes,[7,8] ribo-regulators,[9] synthetic toehold switches,[10] and riboswitches[11,12] which function without any requirements for accessory proteins. The use of post-transcriptional regulation provides an additional point of control, allowing fine-tuning of expression rates. Current methods for tuning genetic circuits often achieve this by modification of the promoter and/or the ribosome binding site (RBS).[13−15] These approaches often require iterative cloning and screening to select for the desired regulatory function. The use of small molecule inducible systems such as inducible promoters can be used to circumvent this need, but these systems often suffer from high basal expression.[16]

Riboswitches are naturally occurring RNA structures found in the 5′ UTR of bacterial genes[11] capable of binding a wide array of small molecules,[17−20] including synthetic inducer ligands.[21,22] RNA devices have been engineered and selected to respond to environmental culture conditions such as pH[23,24] and a wide array of noncognate ligands using *in vitro* and *in vivo* selection methods.[25−30] Riboswitches have been employed in directed evolution[31] and metabolic engineering.[32,33] Additionally, riboswitches have been shown to function across a range of bacterial species[34,35] and even in eukaryotic organisms.[36,37]

Riboswitches consist of two functional domains, a ligand binding aptamer, and a signal actuator, termed the expression platform. In the case of translation activating riboswitches,[20,38,39] ligand binding within the aptamer initiates a structural rearrangement of the expression platform by strand displacement of the RBS sequestering (anti-RBS) sequence, leading to RBS release and translation initiation (Figure 1A). A number of studies have attempted to capitalize on this bipartite structure by inserting aptamer domains upstream from terminator stems to generate riboswitches with modified transcription termination functionality.[35,40] Riboswitches provide a number of attractive advantages: (i) heterologous protein
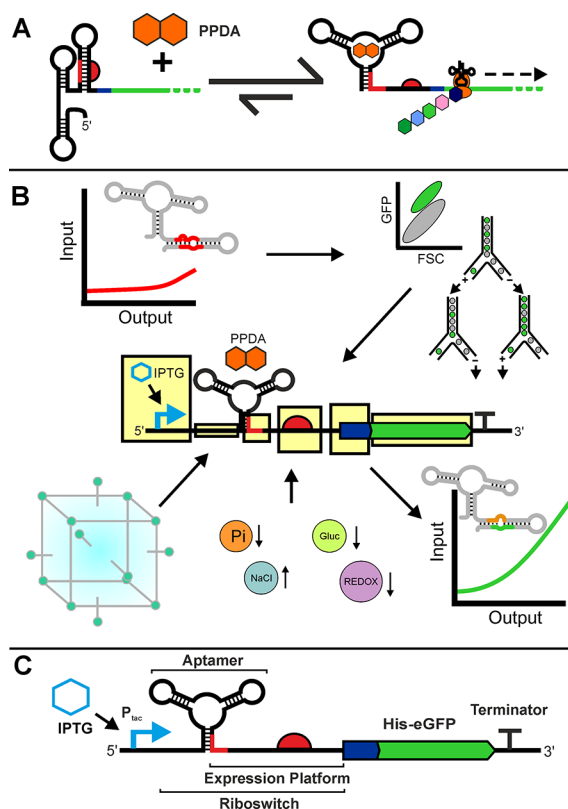
Figure 1. Engineering of the PPDA responsive orthogonal riboswitch for enhanced function. (A) Illustrating the mechanism of the orthogonal riboswitch showing small molecule mediated regulation of protein expression. Protein production is activated in response to pyrimido[4,5-*d*]pyrimidine-2,4-diamine (PPDA), which causes a change in the secondary structure of the eGFP 5′UTR, allowing translation to proceed. (B) An overview of the screening and optimization workflow employed in this study, highlighting the use of *in vivo* FACS selection and design of experiments to improve riboswitch function. This functional enhancement enabled development of four stress responsive riboswitch devices. (C) Schematic overview of a synthetic riboswitch device under regulation of the IPTG inducible P_{tac} promoter showing transcriptional and translational regulation of an N-terminally His tagged eGFP.

expression places a significant burden on the cellular metabolism;[41] therefore, cis-regulation RNA-mediated control of expression reduces cellular burden,[41] as protein production is not required for function.[11] (ii) Additionally, post-transcriptional regulation at the RNA level removes dependence on accessory protein, allowing a rapid regulatory response. (iii) Attenuation of expression levels using a single clone, rather than relying on RBS modification, reduces the need for library development and screening.[42] Taken together, the integration of riboswitches into the 5′UTR should allow the user to quickly obtain dynamic regulation of any given gene of interest.

However, there are a number of additional challenges to the use of riboswitches. Translation initiation from an RBS is influenced by synonymous codon usage of the flanking 5′ coding sequence, and this context dependency has gained a lot attention in recent years,[43,44] with a number of studies using insulator regions and mechanisms to address this problem.[45,46] In addition to this genetic context-dependency, the function of expression systems is also known to be sensitive to contextual changes in environment such as temperature, population density, or metabolic state.[47] To build systems which function

as robustly as possible, it is important to understand how both these genetic and environmental changes can affect protein production and regulatory performance. There are also a number of specific challenges to riboswitch engineering, namely sensitivity of function to the surrounding sequence context.[48,49] In addition, the potential for complex interplay between different riboswitch conformations means predictive molecular engineering is currently challenging.[50,51] In some translational riboswitches such as the adenine binding *addA* riboswitch from *Vibrio vulnificus* and the related pyrimido-pyrimidine-2,4-diamine (PPDA) responsive orthogonal riboswitch (ORS), this is further complicated by overlap of functional regions within the riboswitch at the junction between the RBS sequestering hairpin and the basal stem of the aptamer.[20,35,52] These overlapping regions are essential for the formation of the mutually exclusive OFF and ON structures (Figure 1A) because the RBS sequestering sequence (anti-RBS) is directly involved in formation of the OFF structure.

Previous studies have selected artificial expression platforms to generate functional riboswitches from an aptamer, using fluorescence-activated cell sorting (FACS) and Förster resonance energy transfer (FRET) methods.[53,54] Genetic selection has been applied to improve riboswitch function through expression platform engineering.[27,55] Guided by this work and the riboswitch design rules generated following statistical analysis of *in silico* folding experimental performance metrics,[48] we sought to re-engineer the ORS to achieve high levels of gene expression under conditions of riboswitch activation and to minimize riboswitch expression in the absence of induction while considering the context dependencies which affect RBS riboswitch function.[48,49] To achieve this, we set out to improve performance in a structured and systematic manner using a combination of genetic design variables and environmental factors using Design of Experiments (DoE).

DoE was originally laid out as an essential principle of experimentation.[56] By designing structured experiments, it becomes possible to assess both the effects of factors (genetic and environmental variables, in the case of biology) as well as the interactions between these factors, while efficiently mapping the entire multidimensional landscape of experimental space. DoE has been applied across a range of fields,[57] including bioprocessing[58] and metabolic engineering.[59,60] The complex structure of many designed experiments has previously prohibited the use of DoE within biomolecular engineering for exploration of sequence-function landscapes. With the advent of cheap and accurate DNA synthesis, recent years have begun to see the use of DoE in synthetic biology but with only a few studies exploring sequence level optimization or characterization.[44,61−64]

Here, we describe the use of a high-throughput flow-cytometer-based selection method coupled with DoE for the selection and characterization of the post-transcriptional regulatory RNA devices. This methodology has been used in this study to enhance the function of the ORS. This riboswitch device was selected for development due to its simple structure, relatively modular structure, PPDA solubility, and orthogonality of the ligand from cellular metabolism.[65] We demonstrate that these improved variants afford high levels of translational control across an array of settings and use DoE to explore the sensitivity of riboswitch function to environmental and genetic alterations (Figure 1B). The most robust device was then selected for further testing in a wide selection of genetic contexts.
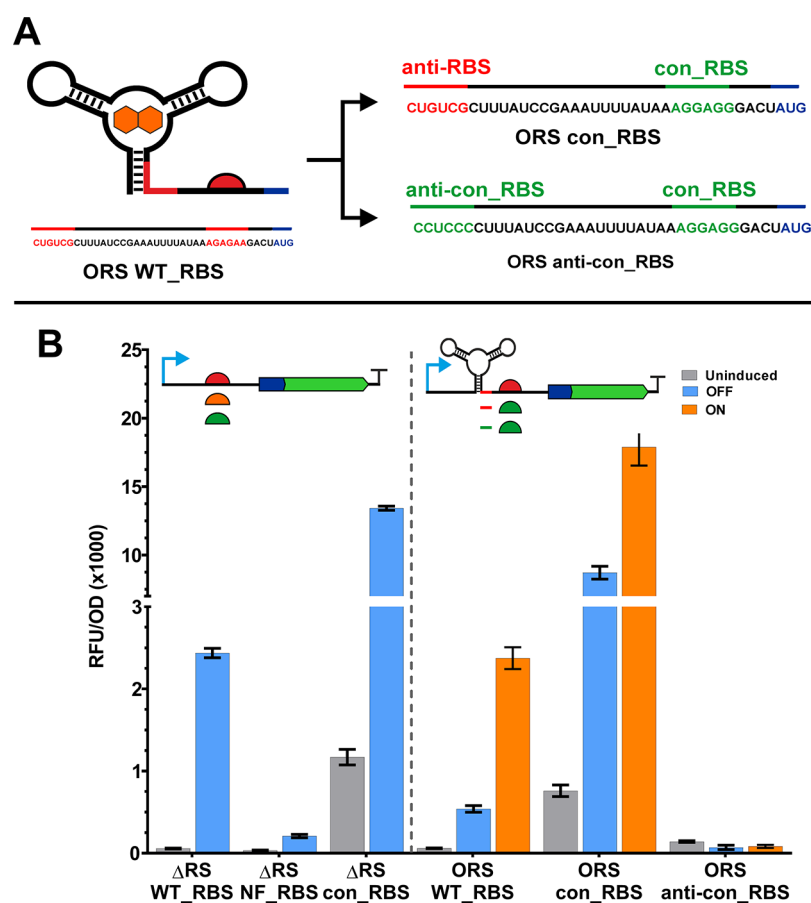
Figure 2. Exchanging the ribosome binding site of the ORS. (A) Overview of expression platform engineering, showing RBS exchange from the native RBS (WT_RBS = AGAGAA, red semi-circle) to the *E. coli* six nucleotide consensus RBS (con_RBS = AGGAGG, green semi-circle), which was expected to improve protein production. Also shown is the ORS anti-con_RBS control sequence which contains the modified anti-RBS sequence. (B) End point measurement of eGFP production following modification of the RBS in constructs lacking the riboswitch aptamer region (left). We first tested the native *addA* WT_RBS under transcriptional regulation from the P_{tac} promoter in the presence (blue) and absence (gray) of IPTG (100 μM). Substitution of the native RBS with a predicted weak/nonfunctional RBS (NF_RBS = TCCTCC) yields greatly reduced protein expression, confirming correct identification of the RBS. Subsequently, the AGAGAA motif was exchanged with the six base consensus sequence (con_RBS = AGGAGG). The right hand side of this graph shows the performance of the ORS with the native and consensus RBS sequences and the ORS_con_RBS with a modified anti-RBS sequence. These constructs were tested in the presence (blue) and absence (gray) of IPTG (100 μM) plus induction of both transcription and translation with IPTG (100 μM) and PPDA (1000 μM) (orange).

■ RESULTS AND DISCUSSION

Previously, we showed that through optimization of N-terminal synonymous codon usage we enhanced riboswitch function.[48] However, although good riboswitch-dependent control was observed, the developed riboswitches exhibited low total expression levels. To further enhance the utility of riboswitches, we set out to achieve vertical extension of the riboswitch-dependent dose response curves by increasing the maximum level of protein production and allowing access to a greater proportion of the total gene expression landscape.

To improve riboswitch function, we aimed to further improve the performance by increasing the translation initiation rate (TIR) when the riboswitch is activated by ligand binding (Figure 1A). In this study, the ORS was placed downstream of the isopropyl β-D-1-thiogalactopyranoside (IPTG) inducible P_{tac} promoter and upstream of an N-terminally His-tagged enhanced green fluorescent protein (eGFP) (Figure 1C). Expression performance was assessed by considering gene expression levels under the following conditions: full riboswitch and promoter induction (ON, 100 μM IPTG and 1000 μM PPDA), expression in the absence of riboswitch induction

(OFF, IPTG 100 μM), and basal expression under uninduced conditions (UI). Riboswitch-dependent control and total gene expression control are determined from the respective ratios ON/OFF and ON/UI. To increase the TIR from the ORS, we modified the region containing the predicted native RBS (AGAGAA), −10 to −4 nucleotide relative to the start codon (Figure 2A)[20] contained with the expression platform region of the riboswitch. We first validated the location of the predicted RBS in the absence of the riboswitch (ΔRS) by mutating the native RBS to the same sequence as the 16S rRNA (TCCTCC) (Methods, Supplementary Table 1), termed the nonfunctional RBS (NF_RBS). Assessment of protein expression from the NF_RBS showed that this alteration greatly affected expression, resulting in very low levels of reporter protein signal when induced with IPTG (RFU/OD = 208) compared to the WT_RBS (RFU/OD = 2436) (Figure 2B and Supplementary Table 2). Following confirmation of the RBS within the ΔRS construct, we exchanged the −10 to −4 nucleotide sequence with the *E. coli* consensus RBS sequence (AGGAGG) (con_RBS).[66,67] The predicted RBS strengths of the WT_RBS and the con_RBS were 811.1 au and 21546.3, respectively (Salis RBS calc. v 2.0).[42,68] Measurement of the
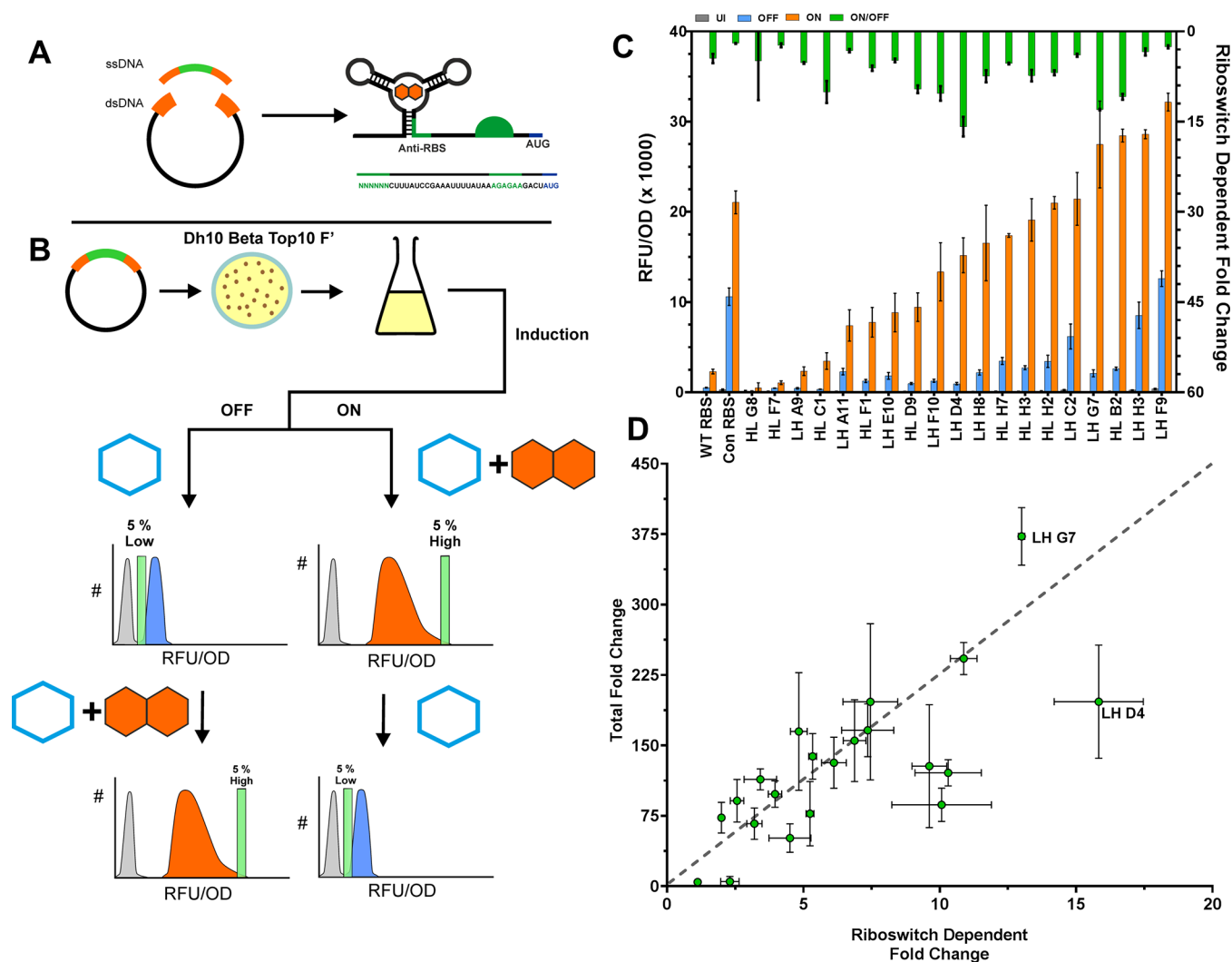
Figure 3. Anti-RBS library and FACS screening. (A) Design and construction of the anti-RBS library. (B) An overview of the FACS screening procedure. This method was used to screen variants of the anti-RBS library for riboswitch function. The library was grown under OFF (IPTG 100 μM, blue) and ON (IPTG 100 μM and PPDA 1000 μM, orange) induction conditions at 30 °C prior to sorting. The lowest 5% of the OFF population and the upper 5% of the ON population was sorted based on eGFP fluorescence intensity (green bow). The sorted populations were recovered and induced under the opposite induction condition, and the alternate sorting procedure was applied, giving two final sorting schemes (low > high, high > low). (C) OFF and ON expression levels (left y-axis) and riboswitch dependent fold change (ON/OFF) (right y-axis) from the 20 functional FACS selected riboswitches following 3 h of induction. (D) Plot showing the trade-off between two important performance metrics ON/OFF and total fold change (ON/UI). LH D4 and LH G7 show the best performance in terms of ON/OFF and ON/UI, respectively. All FACS screened constructs contain His-Linker 30. Error bars represent standard deviation. Data points represent the mean of at least biological duplicate measurements.

reporter protein levels from the con_RBS construct showed high levels of expression compared to WT_RBS and NF_RBS, with an increase of 5.5- and 64.5-fold, respectively (Figure 2B). Following induction with IPTG expression from con_RBS reached 13425 RFU/OD with a dynamic rage (± IPTG) of 11.5-fold, demonstrating that we had successfully been able to achieve a gain of function with substitution of native RBS with the consensus RBS.

In light of the successful increase in TIR, the con_RBS sequence was incorporated into an orthogonal riboswitch-containing construct (Supporting Information and Methods, Supplementary Table 1, and Supplementary Figure 1). Comparison of protein production from the ORS constructs containing the WT RBS (ORS-WT_RBS) and the consensus RBS (ORS-con_RBS) induced with IPTG (100 μM) and PPDA (1000 μM) showed that after 3 h the maximal (ON) expression levels were 7.5-fold higher for ORS-con_RBS. However,

riboswitch-dependent (ON/OFF) control was further reduced from 4-fold to 2-fold (Figure 2B). As a control, we designed an anti-RBS sequence (CCUCCC) with perfect complementary sequence to the consensus RBS (anti-con_RBS) (Supplementary Figure 1C). This showed poor function with very low OFF and ON expression and no PPDA-dependent regulation of expression (Figure 2B).

Riboswitch function is determined by a fine balance between at least two competing RNA structures to afford ON and OFF switching function. Ligand binding causes a conformational change, resulting in a change in stability of the expression platform. The free energies involved in this structural rearrangement have been finely tuned by evolution, making rational design highly challenging.[69] To address these difficulties, we employed a high-throughput FACS-based selection/counter selection methodology to identify riboswitches with optimal OFF and ON states. First, an anti-RBS clonal library with
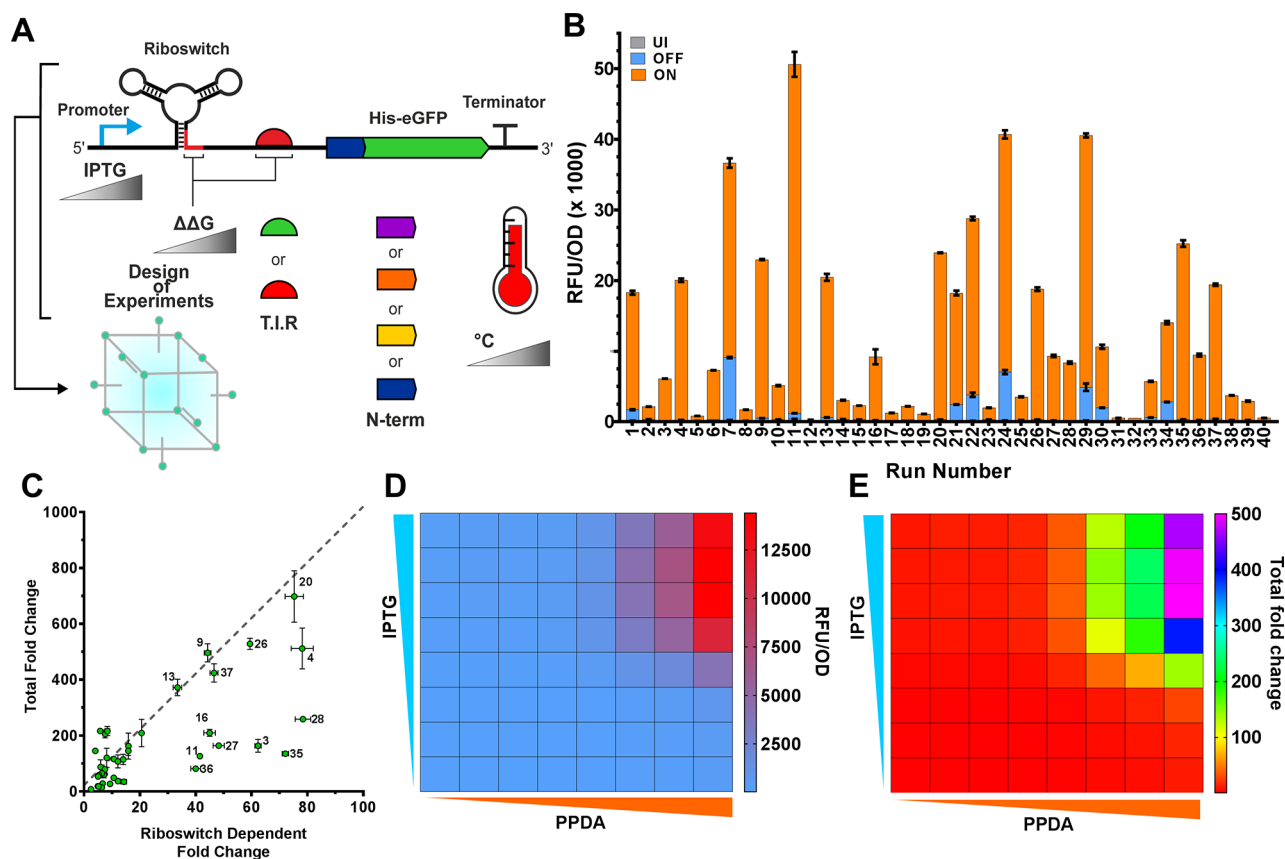
Figure 4. DoE data. (A) An overview of genetic and environmental factors (hairpin $\Delta\Delta G$, RBS strength, N-terminal synonymous codon variant, temperature and IPTG concentration) investigated using Design of Experiments. (B) Measured UI, OFF and ON performance of each riboswitch construct when tested under the factor settings dictated by the D-optimal design (Supplementary Table 5). (C) ON/OFF (x-axis) and ON/UI (y-axis) performance of each tested DOE run. Run number 4 shows the highest riboswitch dependent control. (D) End point eGFP expression testing of D4-ORS-L35 when induced with different concentration of IPTG (1−8, 0, 0.32, 1.6, 8, 40, 200, 400, and 1000 μM, respectively) and PPDA (A, 0, 0.32, 1.6, 8, 40, 200, 400, and 1000 μM, respectively) after 24 h of induction at 37 °C. (E) Calculated total fold change (ON/UI) of the two inducer titration analysis. All error bars represent standard deviation, and data points represent the mean of three technical replicates (B) or biological replicates (D and E).

degenerate nucleotides at positions −36 to −31 was generated by isothermal assembly using a synthetic ssDNA input library (4^6 possible variants) (Methods) (Figure 3A). The library was screened with two rounds of FACS using selection and counter selection (±PPDA) to isolate clones with enhanced riboswitch-dependent control (Methods) (Figure 3B, Supplementary Figure 2).

Following FACS selection, 180 colonies were screened for function after induction with IPTG (100 μM) ± PPDA (200 μM) for 3 h (single replicate only, Supplementary Figure 3). Of these, the 20 best performers were taken forward for sequencing and further expression testing. FACS screening of the anti-RBS library successfully yielded riboswitches with a wide range of function (Figure 3C). A 223-fold range of ON performance was observed with relative expression values between 104 RFU/OD for HL-H3 to 23271 RFU/OD for LH-F9 (Figure 3C, left y-axis). In addition, a diverse range of riboswitch dependent fold change (ON/OFF) was observed (3 h induction, 30 °C) with clones displaying no riboswitch-dependent control (HL-H3) up to 16-fold (LH-D4) (Figure 3C, right y-axis). This riboswitch-dependent control is a significant improvement in both performance relative to the original riboswitch (ORS-WT_RBS), the riboswitch containing the consensus RBS (ORS-con_RBS), and the riboswitch with the consensus RBS perfect complementary anti-RBS sequence (anti-con_RBS)

which displayed 4.4-fold, 2.0-fold, and 1.3-fold, respectively. Coupled with the increased expression level, this gain of function greatly improves the function of the ORS.

The isolation of these riboswitches demonstrates the utility of the FACS sorting protocol for selecting a diverse range of functional riboswitches. Further comparison of riboswitch dependent fold change (ON/OFF) and total fold change (ON/UI) function for all functional FACS selected variants showed that the two best performers for ON/OFF and ON/UI were LH-G7 and LH-D4 (D4-ORS) (Figure 3D). Sanger sequencing of the functional variants was performed, and structural prediction analysis of the D4-ORS was performed (Supplementary Figure 1D). The anti-RBS sequences and expression performance of each variant can be found in Supplementary Table 3. To rationalize, predict, and perform forward molecular engineering of riboswitches with enhanced dynamic range, it is important to understand the respective ON and OFF conformations. For example, if a given anti-RBS variant binds too tightly to an RBS, then the expression platform may remain in an OFF conformation even when the aptamer is ligand-bound. Similarly, a weakly bound RBS−anti-RBS hairpin may lead to an expression platform that remains in an ON even when the aptamer is not ligand-bound. However, *in silico* prediction of ligand-bound riboswitch conformations remains a significant challenge.

To rationalize the performance of new anti-RBS−consensus RBS variants, they were subjected to *in silico* folding analysis[70] to predict the structural stability of the OFF and ON states of the ORS expression platform. The minimum free energy of the OFF state (ΔG OFF) was predicted using the full-length expression platform and the 5′ of the coding sequence (−45 nt to +60 nt). This sequence was then truncated *in silico* to remove the aptamer region of the riboswitch (−36 to +60 nt) as a proxy for the ON state sequence, in a manner similar to that used in Kent et al.[48] (Methods). By using this sequence, the structural predictions allow interrogation of the expression platform when the riboswitch is in the activated RBS-released state. The minimum free energy was then predicted using RNAfold[70] (ΔG ON) and the difference between the two minimum free energies was then calculated ($\Delta\Delta G$ (kcal/mol) (Supplementary Figure 4A). These features make this an essential region in predicting riboswitch function; by using this *in silico* prediction, we hope to further understand the dynamic interplay between the OFF and ON state of the expression platform. The $\Delta\Delta G$ of each functional variant shows a correlation with riboswitch-dependent control ($r = 0.56$, $P = 7.7 \times 10^{-3}$) (Supplementary Figure 4B).

To further assess the performance of the ORS, D4-ORS, we explored the effect of (i) exchanging the flanking coding sequence, (ii) transcription levels, and (iii) environmental factors. Previously, we demonstrated the context sensitivity of the ORS (ORS-WT_RBS) upon downstream coding sequence through the modification of synonymous codon usage.[48] This previous study revealed that riboswitch-dependent performance was dependent upon and could be rationalized on the basis of calculated structural/stability features of the riboswitch and that a fine balance was required in the relative stabilities of the respective ON and OFF conformations to achieve optimal riboswitch performance. Often when producing proteins it is desirable to modify environmental conditions or factors as well as genetic ones to achieve optimal expression and control, for example, lower incubation temperatures to improve folding of recombinant proteins. Typically, the performance of genetic elements or factors is evaluated under fixed environmental conditions. While this approach may yield constructs which function under these conditions, engineered strains and devices may fail to perform robustly under alternative environmental conditions.[47]

Testing all possible combinations of these factors would be challenging, but by applying a DoE (Methods), we aimed to robustly test and optimize the behavior of the D4-ORS-con_RBS while simultaneously exploring the effect of multiple genetic and environmental factors. The selected factors were: transcription level (IPTG concentration) ($n = 3$), incubation temperature (°C) ($n = 3$), predicted TIR ($n = 2$), predicted anti-RBS:RBS hairpin stability ($\Delta\Delta G$ kcal/mol) ($n = 3$) based on minimum free energies calculated from the anti-RBS−consensus RBS variants (isolated using FACS), and N-terminal synonymous codon usage ($n = 4$)[48] (Figure 4A). Four of the previously identified selected N-terminal codon usage variants were tested with the D4-ORS. The selected codon usage variants were variant linker 30 (L30), linker (L35), linker 36 (L36), and linker 32 (L32).[48] For details on the DoE factor levels and data types, see Supplementary Table 4. The use of the fractional factorial D-optimal DoE facilitated a 5.4-fold reduction (216 experiments to 40) in the required number of experiments. For details on the generated experimental design, see Supplementary Table 5. Ribosome binding site engineering (Figure 3) and *in*

silico analysis (Supplementary Figure 4B) of the best performing FACS variants highlights the importance of balancing TIR modification with the complementarity of the anti-RBS. To allow integration of this design consideration into the DoE, the final genetic factor explored was the $\Delta\Delta G$ of the RBS sequestering structure. By using this *in silico* metric, we were able to treat this design factor as a continuous data type, allowing reduction of the required number of experimental runs.

Data for the structured experimental design of reporter protein production was collect after 24 h (Methods). This data shows a large distribution in uninduced (UI), OFF and ON expression levels (Figure 4B). Comparison of the expression data shows that the factors tested greatly affect the riboswitch-dependent fold change (ON/OFF) and total fold change (ON/UI) in expression, changes in ON/OFF ranging from 2.5- up to an impressive 78.1-fold, and ON/UI control between 7.9- and 698-fold. Initial investigation of the optimal expression conditions show that plotting ON/OFF against ON/UI (Figure 4C) shows that run #20 yields the best trade-off between these two responses, while #4 and #20 show similar ON/OFF performance. However, #4 shows a reduced total fold change (ON/UI = 512).

To allow improved investigation and understanding of the multidimensional data set generated from the DoE, a standard least squares (SLS) regression model was fit to the multifactorial expression data set (Methods). ANOVA was used to assess the importance of each factor in the model; significant effects and interactions were selected based on the Log worth statistic, and unimportant factors were removed from the model (Supplementary Table 6). This refined model facilitated deeper investigation into the effects of multiple factors on the four response metrics (OFF, ON, ON/OFF, and ON/UI). The SLS regression highlights the first order effects and second order interactions, which are significant in explaining each of the four responses (Supplementary Table 7). This modeling allows us to formalize several interesting observations about riboswitch expression dynamics.

The generated explanatory model showed that across all four responses, the highly significant ($P < 5 \times 10^{-4}$) factors and interactions were the ON/OFF stability ($\Delta\Delta G$) of the anti-RBS-RBS hairpin, the interaction between TIR and hairpin $\Delta\Delta G$, TIR, and IPTG concentration (Supplementary Table 6). Several other interactions were also significant ($P < 0.01$) (Supplementary Table 6). To test the explanatory power of this statistical model, the prediction for each response was plotted against the actual performance (Supplementary Figure 5), showing that the explanatory model fits the data set well (OFF $P = < 1 \times 10^{-4}$, $r^2 = 0.87$, root mean squared error (RSME) = 883.7; ON $P = < 1 \times 10^{-4}$, $r^2 = 0.86$, RSME = 6140.3; ON/OFF $P = < 1 \times 10^{-4}$, $r^2 = 0.93$, RSME = 8.0; ON/UI $P = < 1 \times 10^{-4}$, $r^2 = 0.85$, RSME = 77.7).

Once the explanatory power of the model had been shown, we set out to investigate the multidimensional, multiresponse data set using the model projections of each respective response. By setting the desired response optimization criteria (minimize OFF expression and maximize ON expression, ON/OFF, and ON/UI, Supplementary Figure 6) interrogation of the standard least squares regression reveals factors with optimal OFF, ON, ON/OFF, and ON/UI performance. Details of the model coefficients for each factor used to build the refined model and the effect of these factors on the individual response variables can be found in Supplementary Table 7. As expected, RBS strength has a significant impact upon both the OFF ($P = 2.8 \times$
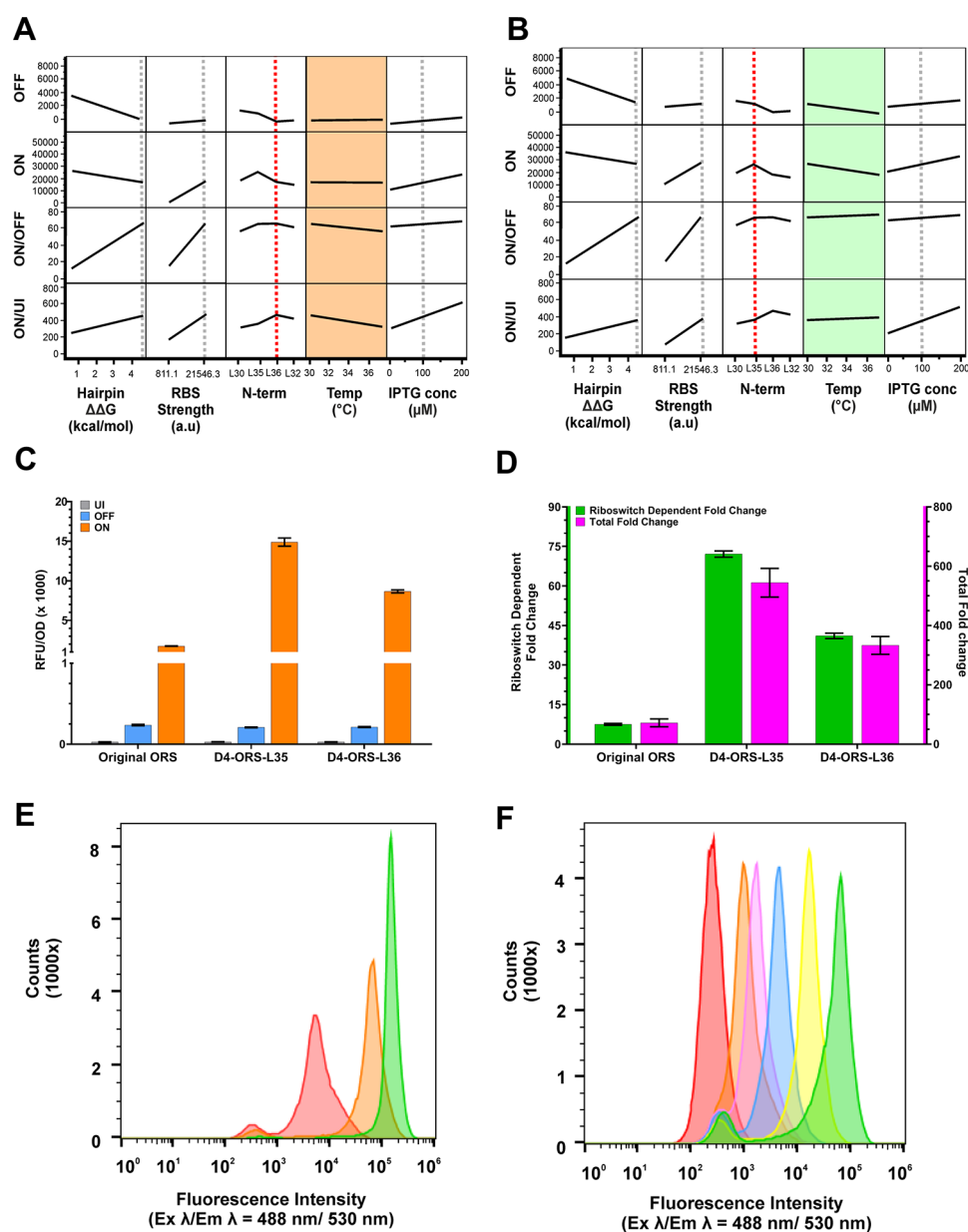
Figure 5. DoE explanatory model showing the effect of the temperature−N-terminal interaction. Standard least squares modeling of the DoE dataset. Model projections showing the effect of hairpin $\Delta\Delta G$, RBS strength, N-terminal His tag, incubation temperature, and IPTG concentration when using the D4-ORS-L36 (A) and D4-ORS-L35 (B). (A) D4-ORS-L36 ON/OFF and ON/UI show an interaction with incubation temperature, as indicated by the slope of the projections in the orange boxes. (B) D4-ORS-L35 ON/OFF and ON/UI shows very little interaction with incubation temperature, as indicated by the reduced slope of the projections in the green boxes. (C) Direct comparison of UI (grey), OFF (blue), and ON (orange) performance of the original ORS construct prior to RBS-anti-RBS modification and DOE optimization and the optimized D4-ORS-His-L30. (D) Comparison of the ON/OFF (green) and ON/UI (pink) of the original ORS riboswitch, D4-ORS-L35, and D4-ORS-L36. Expression data (C−D) was collected from biological triplicate induction assays carried out at 37 °C after 24 h following induction with 100 μM IPTG in the presence and absence of 1000 μM PPDA. (E) Histogram of eGFP fluorescence intensity from ΔRS_conRBS-L35 analyzed by flow cytometry, showing the population distribution of single-cells when induced with different level of IPTG (red = uninduced, orange = 10 μM IPTG, green = 100 μM IPTG). (F) Flow cytometry analysis of the D4-ORS-L35 device following various induction conditions (Red = uninduced, orange = 100 μM IPTG, magenta = 100 μM IPTG + 8 μM PPDA, blue = 100 μM IPTG + 40 μM PPDA, yellow = 100 μM IPTG + 200 μM PPDA, magenta = 100 μM IPTG + 1000 μM PPDA).

10^{-7}) and ON ($P = 1.5 \times 10^{-10}$) expression levels with the strongest RBS (con_RBS) affording a large increase in ON (Supplementary Table 7). Increasing IPTG concentration also has a significant positive effect on both OFF ($P = 4.6 \times 10^{-4}$) and ON ($P = 4.6 \times 10^{-5}$), leading to an increase in both responses with a larger effect upon ON expression than OFF (Supplementary Figure 6). Interestingly the model predicts that both RBS strength and hairpin $\Delta\Delta G$ have a significant positive

effect upon riboswitch dependent control (RBS strength $P = 7.6 \times 10^{-10}$, hairpin $\Delta\Delta G$ $P = 2.0 \times 10^{-10}$) (Supplementary Figure 6, blue boxes). The interaction between these two factors also has a significant effect on ON/OFF function ($P = 5.2 \times 10^{-10}$) and significantly increase total fold change (RBS strength $P = 1.0 \times 10^{-6}$, hairpin $\Delta\Delta G$ $P = 7.2 \times 10^{-4}$). Together, these factor effects suggest that the improved riboswitch function is a byproduct of increasing ON expression while also reducing OFF
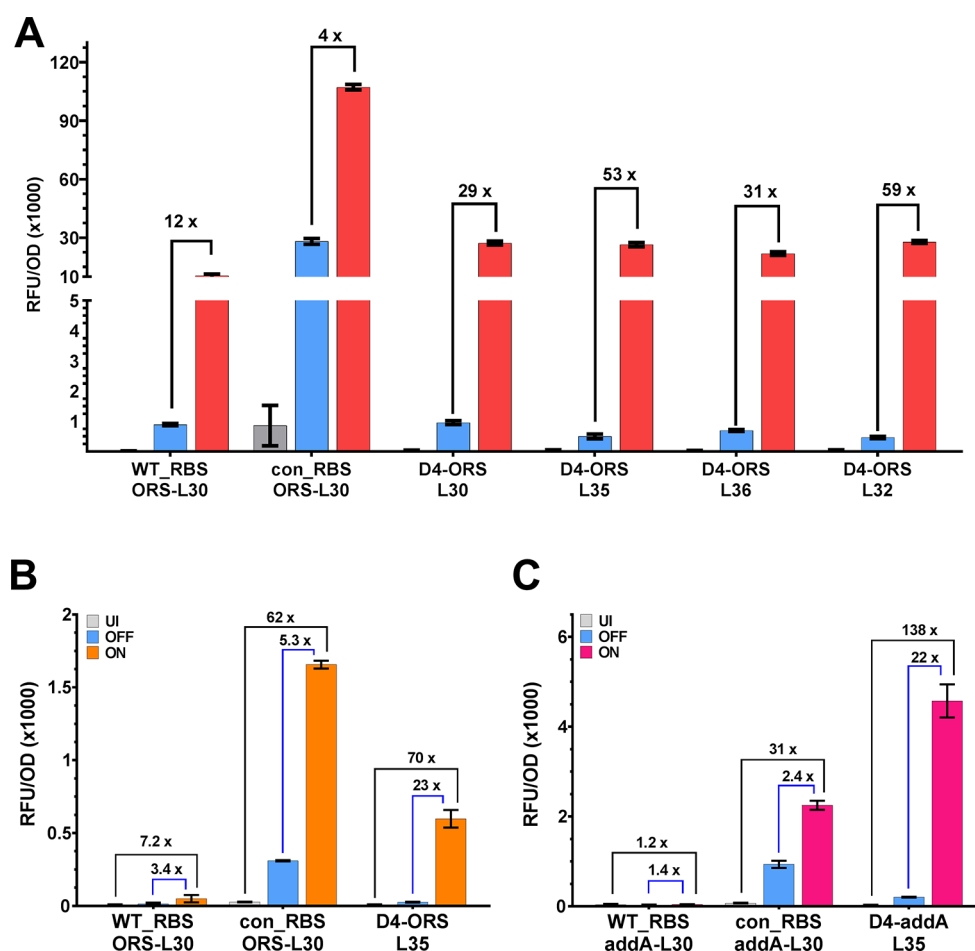
Figure 6. Regulation of plasmid-based mKate2 expression and chromosomally integrated eGFP. (A) Measurement of end point expression (UI = gray, OFF = yellow, ON = red) shows robust riboswitch performance of D4-ORS-L35 and comparison of each N-terminal variant when regulating mKate2 expression. (B) Following genomic integration of the D4-ORS-L35 device into the genome of *E. coli* DH10 beta Top10 F′, the device showed strong ON expression and high fold-change performance values compared to the original ORS construct (100 μM IPTG and 1000 μM PPDA) (ON/OFF = blue brackets, ON/UI = black brackets). (C) Genome integration of the D4-addA riboswitch show greatly improved ON, ON/OFF (blue brackets), and ON/UI (black brackets) performance compared to the original addA riboswitch (100 μM IPTG and 1000 μM 2-aminopurine). Bars represent mean of three biological triplicates; error bars show standard deviation.

and UI expression through proper formation of the anti-RBS hairpin OFF state.

A number of other interacting factors impact OFF and ON expression levels. The concentration of IPTG used shows an additive effect on both OFF and ON expression when used with the stronger RBS (OFF $P = 5.9 \times 10^{-3}$, ON $P = 4.8 \times 10^{-3}$), meaning that when a stronger RBS is used, the effect of IPTG induction is enhanced, leading to higher expression both in the absence and presence of riboswitch activation. Increasing hairpin stability ($\Delta\Delta G$) leads to a reduction in the impact of the IPTG effect on OFF expression ($P = 4.1 \times 10^{-3}$), which means a more stable hairpin reduces the leaky expression from the unactivated riboswitch (Supplementary Table 7). Intuitively, this observation seems to indicate that leaky expression from the riboswitches is caused by nonoptimal anti-RBS hairpin formation in the absence of the ligand (i.e., too weak/low $\Delta\Delta G$), and that by increasing the $\Delta\Delta G$ of the hairpin, this leaky expression can therefore be reduced even at higher levels of transcription. Additionally, RBS strength and hairpin $\Delta\Delta G$ significantly interact, effecting both OFF ($P = 5.6 \times 10^{-7}$) and ON ($P = 1.0 \times 10^{-2}$) expression with the larger effect on OFF expression, suggesting that the importance of proper anti-RBS hairpin formation is greater when a strong RBS is used. In more

practical terms, this means that any transcript which forms a ligand-bound ORS riboswitch structure produces greater levels of eGFP when translation is regulated by the strong consensus RBS.

The set of experimental conditions that best satisfy all four response criteria is DoE run #20 (Figure 4C, Supplementary Figure 6). The plasmid construct used in this run consists of the D4-ORS riboswitch, N-terminal linker L36, induced with 200 μM IPTG at 30 °C. With these parameter settings, the model achieves an optimal balance between OFF, ON, ON/OFF, and ON/UI. However, the model suggests an interesting, albeit small, interaction between two factors. We see that the N-terminal linker L36 has a significant effect on this performance metric, but only when we consider it as part of an interaction with the incubation temperature ($P = 3.0 \times 10^{-2}$). The effect of this predicted interaction was initially investigated *in silico* by modification of the experimental parameter settings to study the effect of this predicted interaction upon riboswitch function (Figure 5). We see that when linker L36 (Figure 5A) is used in the model, projections show an effect of temperature, with a higher incubation temperature having a negative effect on ON/OFF and ON/UI performance. While the predicted ON/OFF and ON/UI of the D4-ORS-L36 is largely unchanged when
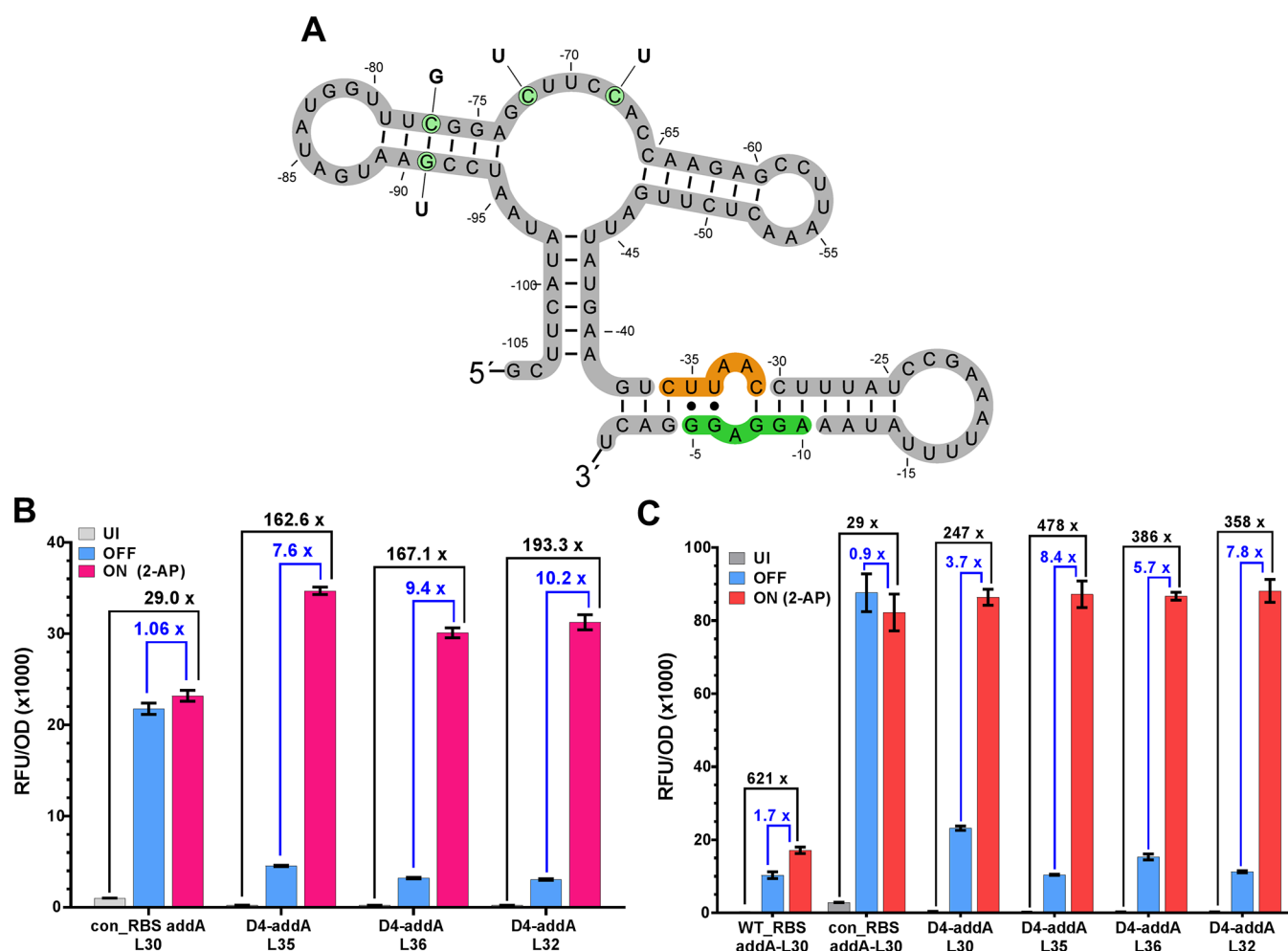
Figure 7. ORS−addA mutation. (A) Predicted structure (RNAfold) of the D4-ORS riboswitch, showing the point mutations responsible for changing ligand specificity (green circles, labeled with mutation) from PPDA to 2-AP, thus restoring the aptamers region of the *addA* riboswitch. The D4 anti-RBS (orange) and consensus RBS are indicated (green); numbering shown is relative to the start codon. (B) 2-AP mediated activation of the addA leads to an increase in protein expression. Blue bars show the level of protein synthesis when induced with IPTG only, whilst green bars show induction with IPTG and 2-AP. The optimized D4 expression platform shows robust performance when the aptamer region is exchanged with the native *addA* aptamer. (C) Performance of the D4-addA devices when regulating the gene expression of for mKate2 (UI = gray, OFF = yellow, ON = red). Error bars represent the standard deviation of three biological replicates. Blue brackets indicate ON/OFF values, whilst black brackets represent ON/UI.

incubated at 30 °C, the real effect of this interaction occurs when temperature is increased to 37 °C. If we instead use the L35 linker with the D4-ORS, then the ON/OFF and ON/UI performance shows a reduced temperature dependency (Figure 5B) with the ON/UI performance being better maintained, irrespective of the induction temperature.

The expression landscape of D4-ORS-L35 in response to both IPTG and PPDA was mapped (Figure 4D), and the total fold change is shown in Figure 4E. This confirmed that D4-ORS-L35 displayed high levels of IPTG and PPDA dependent regulation and displays AND logic behavior with expression requiring the addition of both IPTG and PPDA. An optimal ON/UI of 500-fold was observed with 1000 μM PPDA and 200 μM IPTG. Further investigation of the expression response surface suggested that at 200 μM, IPTG maximal ON expression is achieved, but also that this IPTG concentration leads to an increase in the OFF expression, compared to those cells induced with 40 μM IPTG (Figure 4D). Indeed, at an intermediate IPTG concentration (100 μM) (Figure 5C), D4-ORS-L35 gave consistent ON expression but reduced OFF expression, affording improved ON/OFF performance of 72-fold and

total expression control of 544-fold (Figure 5D). This highlights the need to balance transcriptional and post-transcriptional induction to properly achieve optimal riboswitch performance.

To demonstrate the regulatory improvements achieved, the expression of the optimized constructs (D4-ORS-L35 and D4-ORS-L36) and the original ORS construct (ORS-WT_RBS-L30) (Figure 5C and D) were compared. Fluorescence quantification after 24 h of induction confirmed that the optimized constructs showed drastically improved performance compared to the original ORS construct. The impact of changing the N-terminal linker was then validated by comparing riboswitch performance of the D4-ORS-L36 and D4-ORS-L35 at 37 °C induced with 100 μM IPTG ± 1000 μM PPDA. These results confirmed that D4-ORS-L36 shows reduced performance at 37 °C when compared to D4-ORS-L35.

To assess the expression profile of the D4-ORS construct at a single-cell level, we used flow cytometry to measure cellular eGFP fluorescence. This allowed us to assess the heterogeneity of eGFP expression 24 h after induction with IPTG ± PPDA. Here, we compared the performance of the D4-ORS-L35 with ΔRS-conRBS-L35 (Figure 5E and F). In the absence of any
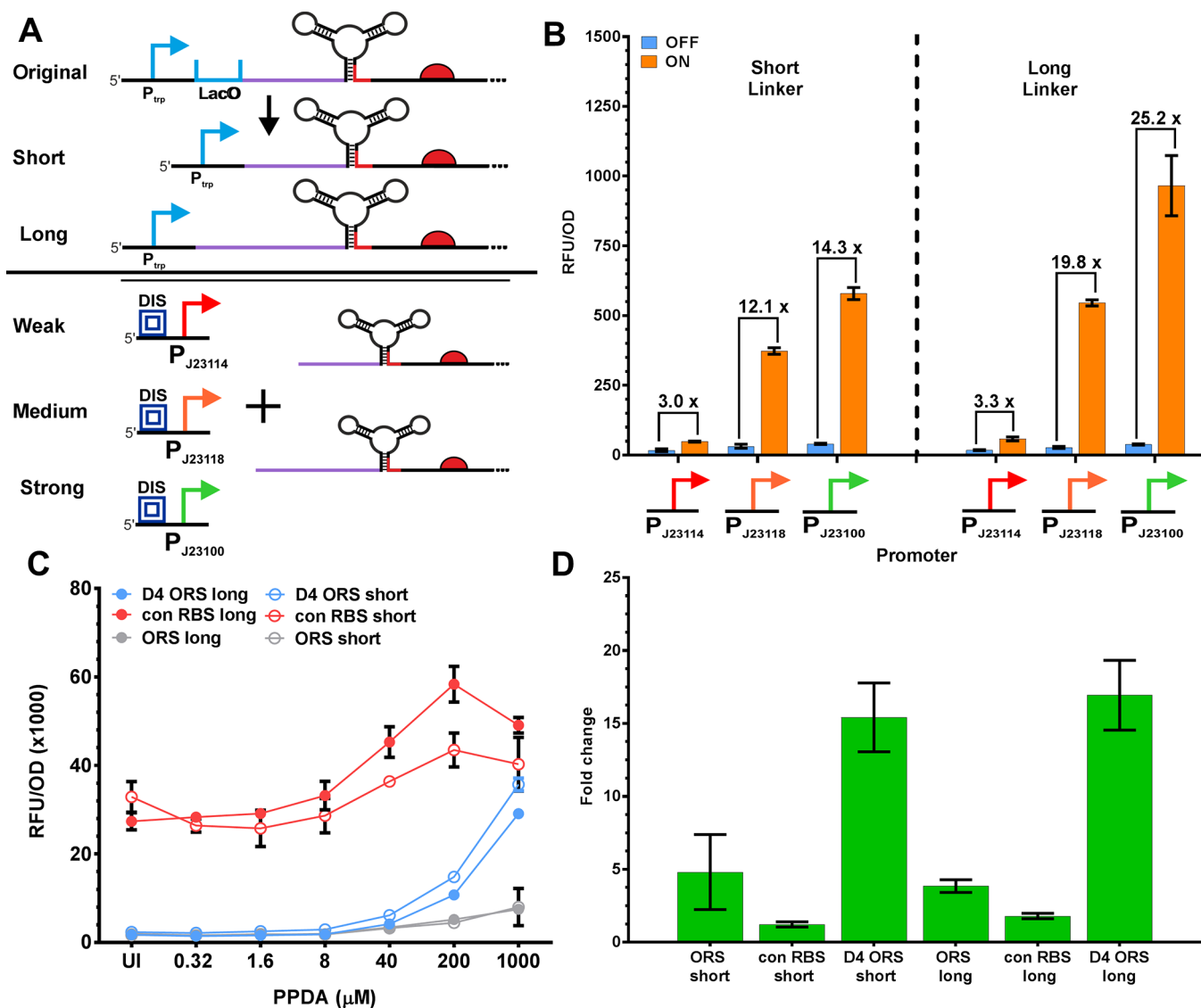
Figure 8. Integrating constitutive promoters into riboswitches allows inducible control of gene expression. (A) Modification of the upstream linker sequence between the transcription start site and the basal stem of the ORS. Deletion of the LacO site from P_{tac} yielded the constitutive P_{trp} promoter with a reduced length transcript upstream of the riboswitch (short). An alternative (long) upstream linker was designed in silico to restore the transcript length to that of the original P_{trp} construct. The P_{trp} was then replaced with three different strength promoters from the Anderson library for further testing. The three Anderson promoter parts (BBa_J23100 (green), BBa_J23114 (red), and BBa_J23118 (orange)) also contained an upstream insulator sequence.[87] (B) End-point measurement of eGFP production from the Anderson promoter regulated devices showing OFF (blue) and ON (orange) performance. The black brackets indicate the level riboswitch dependent control. (C) PPDA titration of gene expression from P_{trp} riboswitch constructs. The performance of the original ORS is shown in gray; the con_RBS ORS is shown in red, and the D4-ORS is shown in blue. Filled circles indicated the long linker, whilst empty circles indicate the short linker. (D) Riboswitch dependent control of each of the P_{trp} constructs.

induction, we see two subpopulations in the ΔRS-conRBS-L35, one with low fluorescence (median = 332 RFU, 7.7% of events) and a second, broad population with higher fluorescence (median = 5661 RFU, 92.3% of events). If we compare this uninduced population with that of the D4-ORS-L35, this shows a single population of cells with low fluorescence (median = 265 RFU). Once induced with IPTG the ΔRS-conRBS-L35 shows strong induction (10 μM IPTG, median = 63 996, IPTG 100 μM 143 785). Upon induction of D4-ORS-L35 with 8, 40, 200, and 1000 μM PPDA and a fixed IPTG concentration of 100 μM, we see titratable regulation of protein production with the median fluorescence measurements from expressing cells reaching 1687 RFU, 4352 RFU, 16 326, and 55 543 RFU, respectively. We also observed a small, low fluorescent

subpopulation following IPTG and PPDA addition, which represents between 7−10% of the total cellular population.

Due to the complexity of interactions between genetic and environmental factors, selection of the best riboswitch design is not as simple as combining the best expression platform with the best N-terminal linker.[48] By identifying the temperature−linker interaction, we selected the final device based on both performance and robustness. This effect would have been difficult to identify using a more traditional "one factor at a time" method, thus supporting our use of a Design of Experiments approach in the multifactorial, multiobjective selection and optimization of this RNA device. For reasons of apparent robustness, the D4-ORS-L35 construct was selected as the best candidate for further evaluation and characterization.

To test the robustness of the D4-ORS-L35 with an alternative gene of interest, we exchanged the eGFP for the alternative reporter protein mKate2 and assayed riboswitch performance (Methods). The D4-ORS riboswitch showed consistently improved performance compared to the original riboswitch with an increase in both ON and ON/OFF (Figure 6A). However, in spite of very similar OFF and ON expression, the D4-ORS riboswitch with an alternative linker L32 performs marginally better when it comes to fold change (ON/OFF = 59) than D4-ORS-L35 (ON/OFF = 53) (Figure 6A). Despite the inconsistent rank performance of the optimal N-terminal linkers when expressing the two different reporter genes, both D4-ORS-L35 and D4-ORS-L32 show high levels of riboswitch-dependent control over the expression of mKate2, making both viable tools for post-transcriptional regulation of protein expression. This performance is vastly improved relative to the original ORS riboswitch that has an ON/OFF performance of just 12-fold and demonstrates that the D4-ORS robustly provides enhanced regulatory performance regardless of the gene being regulated.

It may often be beneficial to integrate regulatory devices into the genome of the chassis to reduce genetic instability caused by plasmid maintenance, and to remove the need to maintain selective pressure through the use of antibiotics. We next wanted to investigate the function of the D4-ORS-L35 riboswitch when inserted into the genome (Methods). The native WT-ORS performs poorly when integrated into the genome, with very low expression levels (UI = 10 RFU/OD, OFF = 19, ON = 49) and poor riboswitch-dependent control (ON/OFF = 3.4-fold) (Figure 6B). However, by using the optimized D4-ORS-L35 we are able to regulate expression of the gene of interest from a single copy present on the genome (UI = 9, OFF = 26, ON = 598), affording riboswitch-dependent and total control over-expression of 23-fold and 70-fold respectively (Figure 6B). By optimizing the function of these riboswitches, it is now possible to use riboswitch from a genomic locus, and obtain high levels of control and tight basal expression. This development greatly expands the utility of the PPDA responsive riboswitch.

To establish whether the optimized riboswitch would provide enhanced function when the aptamer was replaced, we exchanged the ORS aptamer domain for the related 2-aminopurine (2-AP) responsive *addA* aptamer domain from *Vibrio vulnificus* (Figure 7A). When the con_RBS is present, we observe ON expression far higher than previously reported,[48] affording a 29-fold total fold change. However, as expected without the cognate anti-RBS, the OFF expression level is also very high, and poor riboswitch-dependent control is observed. The *addA* aptamer was then assessed with the D4 expression platform and linker (L35, L36, and L32) combinations. These re-engineered *addA* riboswitches show tight basal expression and high ON expression with ON/UI of 162-fold, 167-fold, and 193-fold, respectively. However, while the ON/UI shows good function, the ON/OFF performance of the D4-addA was reduced in comparison to the D4-ORS variants (7.6-, 9.4-, and 10.2-fold for L35, L36, and L32 respectively, Figure 7B). However, this is likely due to elevated OFF expression caused by cognate inducer adenine present in the cell at 97 μmol/mg DCW.[71] The highest ON/OFF of 10.3-fold was observed in the D4-addA-L32. The D4-addA devices were also used to regulate the expression of mKate2 (Figure 7C). The performance of these constructs was similar to that observed when regulating eGFP production, but in this case, the D4-addA-L35 showed the great fold change performance (ON/UI = 476, ON/OFF = 8.4). The engineered performance of the D4 expression platform may

serve as a useful platform for the future development of post-transcriptionally regulated riboswitches through integration of other ligand binding domains.

In addition to testing the D4-*addA* riboswitch on a plasmid, the riboswitch construct was also integrated into the genome of *E. coli* (Figure 6C). Similar trends to the D4-ORS were observed with the consensus RBS greatly increasing ON expression and the D4 anti-RBS leading to restoration of tight UI and OFF expression. The D4-*addA* riboswitch showed riboswitch-dependent control (ON/OFF, 22-fold) very similar to that of the D4-ORS riboswitch. This is a drastic improvement compared to the native *addA* riboswitch (ON/OFF = 1.4). Total fold change (ON/UI) was also greatly increased from 1.2-fold up to 138-fold.

To further explore the context dependency of riboswitch performance and expand their utility as modular control elements for use in synthetic biology, we next looked to examine the dependency upon upstream sequence and promoter. To do so, we initially deleted the LacO sequence of the promoter (P_{tac}) immediately downstream of the transcription start site (TSS) (Methods), reducing the length of the transcript upstream of the basal aptamer stem by 21 nt (Figure 8A). The effect of this reduction in transcript length upstream of the riboswitch was investigated by designing an alternative upstream linker, restoring the original length of this upstream region to that of the P_{tac} system (49 nt). This nucleotide sequence was manually designed to reduce any predicted interaction with the OFF state riboswitch using RNAfold.[70] D4-ORS riboswitch constructs with both the short and long upstream linkers were tested under the control of 3 constitutive promoters across a range of promoter strengths (BBa_J23114 = 0.1 a.u, BBa_J23118 = 0.56 a.u, BBa_J23100 = 1 a.u) using promoters from the Anderson collection[72] (Figure 8A).

Expression analysis with these constructs confirmed that the D4-ORS riboswitch functions robustly under constitutive promoter regulation with riboswitch-dependent control of up to 25-fold observed. We also observed that the rank order of the Anderson promoters was not impacted by the insertion of the riboswitches (Figure 8B). Comparison of the short linker vs the longer linker revealed that the longer upstream linker consistently performed better than those with the short linker both in terms of ON and ON/OFF performance (Figure 8B). The ON performance of the long linker was 20, 46, and 66% higher than the short linker constructs for BBa_J23114, BBa_J23118, and BBa_J23100 promoters, respectively. The effect of modifying the length of the upstream sequence was further expanded by testing both the short and long linker variants when place under the control of the strong P_{trp} promoter (Figure 8C). Interestingly, the riboswitch-dependent control of both short and longer linker D4-ORS constructs showed no significant difference, and the discrepancy between linker length was reduced in comparison to that observed when transcription initiation was regulated by the weaker Anderson promoters.

The importance of the upstream sequence explored here highlights this as another important factor to consider when incorporating these *cis* post-transcriptional regulation devices into any genetic control element. Importantly, incorporation of the riboswitches showed that simply by incorporating 154 nt into the 5′ UTR of a selection of constitutive promoters, we obtained inducible expression control units with riboswitch-dependent control of up to 25-fold, demonstrating the use of the D4-ORS riboswitch to convert constitutive promoters into small
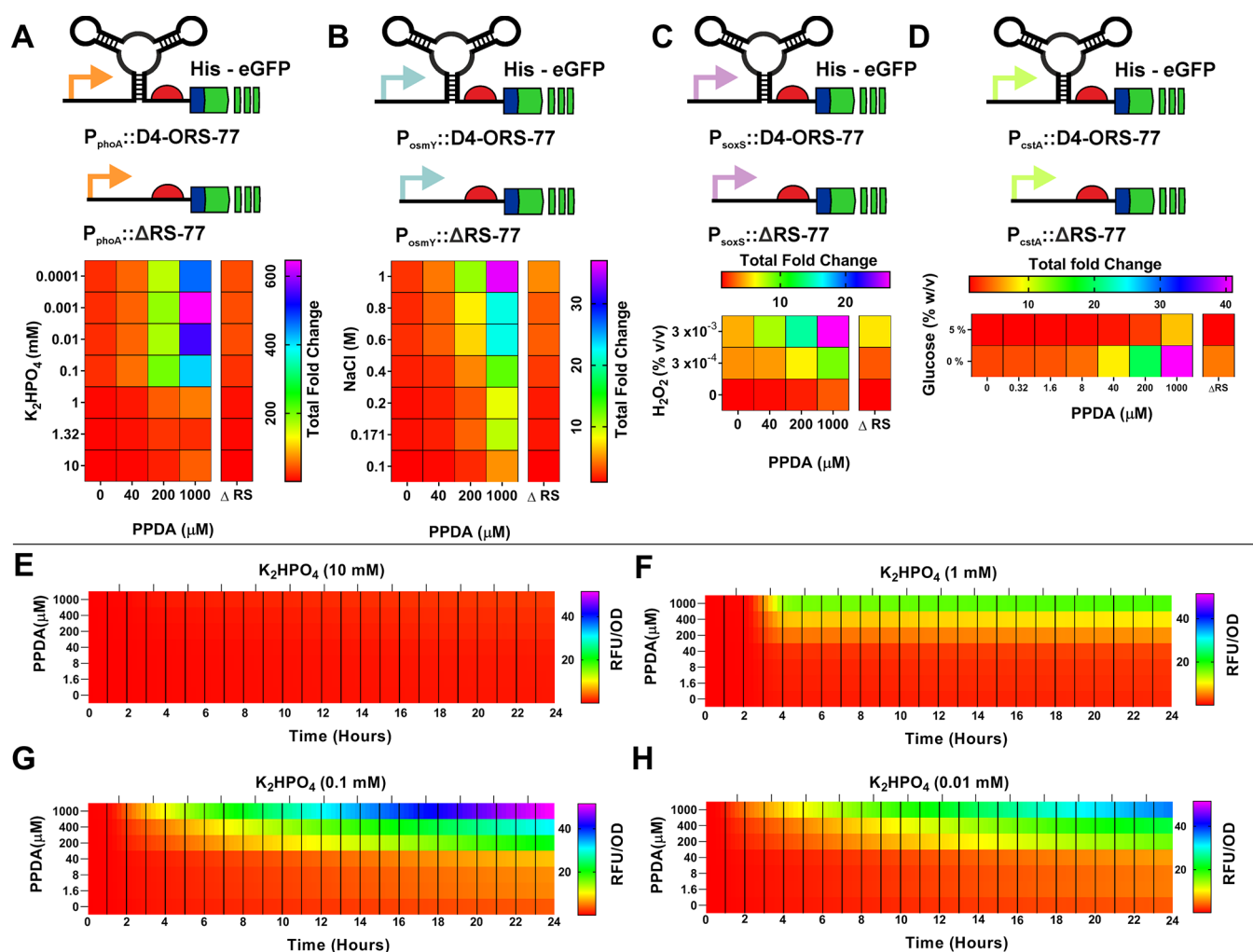
Figure 9. Integration of orthogonal, post-transcriptional regulation into endogenous stress response pathways. Induction matrix heat maps showing the observed ON/UI for the P_{phoA} (A), P_{osmY} (B), P_{soxS} (C), and P_{cstA} (D) D4-ORS-L35 devices following different levels of transcriptional and post-transcriptional induction with PPDA and K_2HPO_4, NaCl, H_2O_2, or glucose starvation. ΔRS controls included for comparison. E–H show kinetic microfermentation characterization of eGFP production (RFU/OD) from the P_{phoA}::D4-ORS-L35 devices when grown in EZ-rich media supplemented with varying levels of K_2HPO_4 (E = 10 mM, F = 1 mM, G = 0.1 mM, H = 0.01 mM) over 24 h. Data represent the mean of three replicates. Raw data and standard deviations can be seen in Supplementary Table 8.

molecule induced expression units across a range of different promoter strengths. Given that the longer linker gave better or equivalent ON/OFF performance for the constitutive promoters tested, this linker was selected for future testing of additional transcriptional and post-transcriptionally regulated devices. Exploration of the upstream linker region for these constitutive promoters allowed us to standardize this transcript region for future engineering.

Following the successful integration of the D4-ORS-L35 riboswitch downstream from a series of constitutive promoters, we looked to integrate the D4-ORS-L35 into a variety of endogenous environmentally regulated, stress response promoters. A number of recent studies have developed stress responsive, transcriptionally regulated devices.[73,74] While systems which utilize cellular stress to induce transcription provide a real time response to metabolic stress, the strength of this response cannot be dynamically regulated. By integrating post-transcriptional regulation downstream of such promoters, it should be possible to couple the stress response elements with small molecule induction and temporal control. Another common mechanism for regulating gene expression is through

the use of bacterial starvation responses. Post-transcriptional regulation provides an interesting opportunity to advance the use of systems such as the phosphate starvation promoter, which has been used in the biological manufacture of therapeutic proteins.[75] In this case, the only way to modify the strength of the starvation response upon gene expression is to engineer elements such as the RBS. By integrating such promoters with riboswitch device, we can modulate the magnitude of gene expression to optimize the production of the desired protein of interest. By replacing the original promoter (P_{tac}) with a number of environmental and metabolic stress response promoters, namely hyperosmotic stress (P_{osmY}), phosphate starvation (P_{phoA}), redox stress (P_{soxR}), and carbon starvation (P_{cstA}) responsive promoters (Methods, Supplementary Table 1), we constructed tools which are regulated by both the respective stress response and the riboswitch ligand concentration.

In Figure 9A, we see that the no-riboswitch control (ΔRS) P_{phoA} promoter is responsive to K_2HPO_4 over the concentrations assessed (10 to 0.0001 mM), affording expression output over a 38.6-fold range. For the P_{phoA}-D4-ORS, we see that the expression is controlled in response to both varying K_2HPO_4

and PPDA concentrations (Figure 9A). The greatest ON is observed at 0.001 mM K_2HPO_4 and 1000 μM PPDA, while in the absence of PPDA, we observe tight control of basal expression regardless of the initial phosphate concentration (gray, Supplementary Figure 7A). Riboswitch-dependent control of expression of up to 48-fold was observed under 1000 μM PPDA and 10 mM K_2HPO_4 conditions. A maximal PPDA and K_2HPO_4 dependent dynamic range of the P$_{phoA}$::D4-ORS-eGFP device was 646-fold, observed for 1000 μM PPDA and 0.001 mM K_2HPO_4 with both PPDA and phosphate dependent regulation of expression (Figure 9A). This is a significant increase in the dynamic range of this promoter compared to when no riboswitch is present. Despite the reduction in maximal ON expression, this enhanced dynamic range is achieved by drastically reducing the basal "leakiness" of the promoter under high phosphate conditions.

Similar trends were observed for the P$_{osmY}$::D4-ORS-eGFP. This system was induced by both hyperosmotic stress and PPDA (Figure 9B, Supplementary Figure 7B), and GFP fluorescence was measured after 3 h of hyperosmotic stress and PPDA induction. Tight control of basal expression, regardless of the NaCl concentration, is afforded by riboswitch integration (Figure 9B). The maximal ON expression level was reached at 1 M NaCl and 1000 μM PPDA with riboswitch performance of 7.3-fold and ON/UI of 36-fold (Figure 9B, gray Supplementary Figure 7B). In comparison, the P$_{osmY}$ ΔRS construct showed NaCl dependent induction of gene expression with only 4.9-fold control. The P$_{osmY}$ is also active under stationary phase as well as being induced by osmotic stress.[76−78] To investigate whether the expression of eGFP during stationary phase could be regulated by the riboswitch, we also measured eGFP expression after 24 h (Supplementary Figure 8). At this time point, we see a loss of osmotic stress dependent expression in the P$_{osmY}$::D4-ORS strain; in fact, expression is reduced at very high NaCl concentrations (0.8 and 1 M) in the P$_{osmY}$ ΔRS construct, likely due to inhibition of cell growth. Despite loss of NaCl dependent modulation of protein production, riboswitch-dependent control of expression was maintained with PPDA dependent regulation up to 15-fold (ON/OFF) after 24 h, showing that the D4-ORS is able to regulate expression independently of both osmotic stress and stationary phase dependent effects.

Another stress response transcription factor dependent promoter was coupled to the D4-ORS-L35 and assessed for its ability to respond to peroxide stress. Comparatively, the P$_{soxS}$::D4-ORS-eGFP device displayed H_2O_2 dependent expression after 3 h of expression when induced with a range of H_2O_2 and PPDA concentrations. At 3 h, expression was altered in response to increasing both H_2O_2 (% v/v) and PPDA concentration (Supplementary Figure 7C). The ON/UI for the P$_{soxS}$ reached 26.8-fold (0.03% H_2O_2, 1000 μM PPDA) (Figure 9C). P$_{soxS}$ and the soxRS have recently been used for sensing imbalance of $NADP^+/H$ redox state,[79] giving the P$_{soxS}$::D4-ORS-L35 device great potential in optimizing redox dependent pathways in biotechnology.

The final stress responsive riboswitch device constructed utilized the carbon starvation promoter P$_{cstA}$. This strong stationary phase promoter is σ70 regulated and glucose repressible. Following cAMP accumulation, CRP positively regulates P$_{cstA}$ activity, leading to transcription initiation. Following expression analysis in LB $\pm$ 5% glucose, we observed that the P$_{cstA}$::ΔRS is positively regulated in the absence of glucose, which corresponds to a 4.4-fold increase in eGFP production when cells are cultured in the absence of glucose.

The same trend in observed upon integration of the D4-ORS; as expected, this device shows riboswitch-dependent control (Figure 9D, Supplementary Figure 7D). Glucose dependent expression control in the D4-ORS device reached 7.2-fold (at 200 μM PPDA), and PPDA addition led to a 9.5-fold increase in protein synthesis. Combined, the effect of glucose starvation and PPDA induction yielded an ON/UI of 34.8-fold change in eGFP production (Figure 9D) on induction with 1000 μM when induced by carbon starvation.

In summary, riboswitch-dependent control of the output signal from bacterial stress response promoters proved successful, and Figure 9 shows that each promoter was activated by the respective stimuli. By integrating D4-ORS into these endogenous promoters we have been able to decouple the signal processing of these cellular stress responses through post-transcriptional regulation. The introduction of a riboswitch into these promoter elements converts the simple input-output system into a two-input system, as both stress response promoter and riboswitch activation (stress + PPDA) is required to give an output (eGFP expression).

In addition to production applications, these tools could be of use as sensors in developing understanding of cellular stress responses and metabolic and environmental stress. Coupling of stress response promoter with post-transcription, RNA regulated, small molecule inducible control of expression provides an interesting opportunity. This system allows cellular detection of a given stress stimuli, meaning that when this stress exceeds the limits deemed acceptable by the cell (selective pressure), transcription occurs. However, the riboswitch will adopt the OFF conformation until user addition of PPDA, allowing tunable, temporal control over the strength of the cellular stress response.

Following the end-point characterization of the P$_{phoA}$::D4-ORS device, we characterized the expression kinetics of the device in a mini-fermentation system (BioLector, M2P-Laboratories). Expression of eGFP for the P$_{phoA}$ riboswitch device was measured over a 24-h period (Figure 9E−H; Supplementary Table 8). Cells were supplemented with different amounts of K_2HPO4 to allow comparison of eGFP expression in phosphate replete and depleted conditions. When supplemented with 10 mM K_2HPO_4, P$_{phoA}$ is not activated (Figure 9E); however, at 1 mM K_2HPO_4 and below, eGFP production is observed, indicating activation of P$_{phoA}$ (Figure 9F). Expression begins at ∼2 h, indicating the onset of the starvation response and plateaus after 4 h, which coincides with entry into the stationary growth phase (Supplementary Figure 9). When grown in 0.1 mM K_2HPO_4, this expression onset delay is reduced to ∼30 min (Figure 9G), and at 0.01 mM K_2HPO_4, expression is observed upon the initial measurement, suggesting that the cells have entered a starved state directly following resuspension in media at this concentration of K_2HPO_4. At both of these lower K_2HPO_4 levels, we see that eGFP production does not plateau throughout the 24-h measurement period. This is likely due to the severe phosphate limitation, as indicated by the poor growth of these cultures.

At all phosphate concentrations, the basal level of expression is tightly repressed (Figure 9E−H) in the absence of PPDA, and expression is increased in a PPDA-dependent manner, high-lighting the utility of the D4-ORS to tightly control expression even when transcription has been induced. To assess the modification of eGFP production rate upon addition of PPDA, linear regression was carried out during the linear region of the RFU/OD data sets (2.5−3.5 h). The slope coefficients detailing

the effect of PPDA on the eGFP production rate can be seen in Supplementary Table 9. The fastest production rate is observed at 1 mM K_2HPO_4 and 1000 μM PPDA. After 24 h, the maximal eGFP signal is observed in the 0.1 mM K_2HPO_4 culture with 1000 μM PPDA (Figure 9G). However, when cells are starved at a phosphate concentration below this (0.01 mM K_2HPO_4), we see a reduction in the maximal fluorescent signal and rate of expression. This ability to attenuate both the expression levels and rate of expression further expands the utility of both stress induced promoter and riboswitches for protein production applications.

■ CONCLUSION

The findings presented here demonstrate the power of combining functional selection and multidimensional, multi-objective optimization for constructing RNA regulators with improved functionality. We show that through incorporation of both the consensus *E. coli* RBS and an anti-RBS library that subsequent FACS enrichment and selection of riboswitches with optimal anti-RBS hairpins can be achieved. Following further functional optimization through DoE riboswitch, function of the ORS can be greatly improved (820% improvement in ON state expression) with PPDA induced riboswitch-dependent control (ON/OFF) up to 72-fold and overall transcriptional (IPTG) and post-transcriptional (PPDA) regulation across a 544-fold dynamic range (ON/UI) (Figure 5D). Design of Experiments also allowed prediction of factors likely to affect riboswitch robustness using sparse sampling of a large experimental space to enhance understanding, probe complex interactions and environmental factors, and guide optimal construct selection. By improving the function of the PPDA responsive riboswitch, we built a device comparable with the widely used theophylline riboswitch,[53] thus expanding the RNA device toolbox, which will be of great use to the synthetic biology community and reduce dependence upon protein- and transcription-factor-based regulation.

Unsurprisingly, the SLS regression model predicts that the stability of the expression platform hairpin dictates riboswitch function. In future work, we hope that this framework will allow further prediction of switches with further enhanced function. Currently, this has proved challenging due to the complexities of *in silico* structural prediction. A recent review of RNA device design highlights a number of the challenges in this area.[80] It is possible that incorporation of more advanced kinetic or three-dimensional structural predictions into the DoE framework could allow us to build a predictive model. Additionally, the SLS model built here assumes, for simplicity, only linear relationships between factors. While this has proven sufficient for construct selection and robustness testing, nonlinear modeling may facilitate future further improvement of riboswitch function.

We demonstrate that the riboswitch developed here functions robustly in a wide array of contexts, including the regulation of an alternative gene of interest, when inserted on the genome, and downstream of a number of different constitutive promoters. In constructing the devices containing these constitutive transcriptional regulators, we also highlight the importance of the 5′ UTR, the linker region between the TSS and the riboswitch structure. The design of these devices was then used to inform the design of four endogenous *E. coli* stress response promoter riboswitch regulators. The orthogonal riboswitch allows translation control of expression from stress responsive promoters only when PPDA is present. This additional layer of expression control allows exogenous control

of expression following the induction of transcription by the respective environmental metabolic stress. This additional layer of riboswitch-dependent control allows for temporal control and activation of gene expression in response to environmental and stress stimuli.

Decoupling of growth and production phases has been previously implemented to maximize volumetric production titers using both process control strategies such as autoinduction media or late stage fed-batch induction[81,82] and autonomous genetic control.[73,83] However, a challenge with using autonomous control elements such as promoters responsive to environmental or stress stimulus is their undesired activation during preculture conditions and prior to induction. Here, use of a riboswitch permits tight basal control of gene expression in the absence of riboswitch activation, and upon further activation, the expression output is attenuated over a large range. This may prove particularly useful in bioprocessing of toxic or difficult to express proteins, when it is often desirable to accumulate biomass prior to protein production while maintaining tight regulation of expression. This can be challenging in traditional expression systems due to high basal expression and population-level expression heterogeneity. By utilizing post-transcriptional control, these issues can be easily addressed. Additionally, by combining the endogenous sensing capabilities of the cell with riboswitch control, we addressed a major limitation to the use of riboswitches. Currently, the numbers of riboswitch−ligand pairs are somewhat limited, and those which respond to orthogonal small molecule inducers are limited yet further. By tapping into a number of endogenous sensory pathways, we expanded the stimuli, which can regulate protein expression, through post-transcriptional control. In the case of these systems, promoter activation machinery provides stimuli specific induction, and the riboswitch affords tunable control. In other words, once transcription has be activated by the respective stress stimuli, the magnitude of this activation can be regulated by riboswitch addition, allowing the expression rate to be balanced with respect to the cellular capacity to produce, process, or secrete the desired protein of interest.[84] The combination of stress activated transcription and tunable control of protein production will hopefully prove of great use to the synthetic biology and bioprocessing communities.

■ METHODS

Strains and Plasmids. All cloning, including library generation, was carried out using HiFi assembly (NEB #E5520S) and transformation into *Escherichia coli* DH5 alpha (NEB #C2987). Assembly DNA was synthesized either as dsDNA or ssDNA. Plasmid DNA was then isolated using silica column purification (Qiagen) and transformed into chemically competent *E. coli* DH10β Top10 F′ (ThermoFisher Scientific). This strain was used for all subsequent expression analyses, unless stated otherwise. pKIKO vectors were cloned in *E. coli* PIR2 strain (Invitrogen). For details on cloning, see Supporting Information and Methods. The sequence of the pTAC-ORS-L30-eGFP plasmid and key expression cassettes, consisting of the promoter-5′UTR-CDS-terminator region of the main devices used in this study, can be found in Supplementary Table 10.

Cultivation and Expression Conditions. Single colonies were inoculated into LB medium and carbenicillin 100 μg mL^{-1} (0.5% yeast extract, 0.5% NaCl, 1.0% bactotryptone) following calcium chloride mediated transformation of plasmid DNA into chemically competent cells prepared according to a modified

procedure.[85] Liquid cultures were incubated at 37 °C with shaking at 200 rpm for 16 h overnight. These seed cultures were diluted 100× in 10 mL of LB supplemented with 0.2% glucose and incubated as before for 2 h (OD 600−0.3). Cultures were then aliquoted (500 μL) into deep well plates (Amgen 1.4 mL 96 well plates) with the designated final inducer concentrations (100 μM IPTG) and pyrimido-[4,5-d]-pyrimidine-2,4-diamine (PPDA) or 2-amino- purine (2-AP) at 1000 μM for standard OFF−ON expression. All constitutive promoter constructs were induced with PPDA only, i.e. no IPTG was required. Following incubation for 3 h, 250 μL of culture was aspirated into a separate deep well block, and cells were harvested by centrifugation. Cell pellets were then washed with PBS (Sigma), diluted 1:4, and the cell density and fluorescence were recorded using a ClarioStar microplate reader (BMG).

EZ-rich media (Teknova) was used for testing and kinetic characterization of the PphoA::D4-ORS-L35 device. EZ-rich is a modified Neidhardt media[86] with the following composition: 40 mM MOPS, 4 mM tricine, 0.01 mM iron sulfate, 9.5 mM ammonium chloride, 0.276 mM potassium sulfate, 0.0005 mM calcium chloride, 0.525 mM magnesium chloride, 50 mM sodium chloride, 3×10^{-9} M ammonium molybdate, 4×10^{-7} M boric acid, 3×10^{-8} M cobalt chloride, 10^{-8} M cupric sulfate, 8×10^{-8} M manganese chloride, 10^{-8} zinc sulfate, 1.32 mM potassium phosphate, 1.5 mM potassium hydroxide, 0.2 mM adenine, 0.2 mM cytosine, 0.2 mM uracil, 0.2 mM guanine, 0.8 mM L-alanine, 5.2 mM L-arginine HCL, 0.4 mM L-asparagine, 0.4 mM L-aspartic acid (potassium salt), 0.6 mM L-glutamic acid (potassium salt), 0.6 mM L-glutamine, 0.8 mM L-glycine, 0.2 mM L-histidine HCL H$_2$O, 0.4 mM L-isolucine, 0.4 mM L-proline, 10 mM L-serine, 0.4 mM L-threonine, 0.1 mM L-tryptophan, 0.6 mM L-valine, 0.8 mM L-leucine, 0.4 mM L-lysine, 0.2 mM L-methionine, 0.4 mM L-phenylalinine, 0.1 mM L-cysteine HCL, 0.2 mM L-tryosine, 0.05 mM thiamine, 0.01 mM calcium pantothenate, 0.01 mM para-amino benzoic acid, 0.01 mM para-hydroxy benzoic acid, 0.01 mM dihydroxyl benzoic acid, and 0.2% glucose (w/v).

FACS Counter-Selection of Improved Riboswitch Variants. Two separate sorting schemes were applied to isolate functional riboswitches from the anti-RBS library; sorting of cells with low fluorescence intensity under OFF induction, followed by sorting of highly fluorescent cells under ON induction (low > high). Conversely, the opposite scheme was also applied, where highly fluorescent cells were sorted under ON induction, followed by isolation of cells with low fluorescence when induced with OFF. Prior to FACS sorting, 500 μL of the cryopreserved library was inoculated into 50 mL of LB + carbenicillin 100 μg mL^{-1} and incubated for 16 h at 30 °C with shaking at 200 rpm. The culture was diluted 100× and incubated as before for 2.5 h (OD600 = 0.3). Cells were then induced with either 100 μM IPTG or 100 μM IPTG + 200 μM PPDA and incubated for 20 h at 30 °C, and cells (2 mL) were then harvested by centrifugation and resuspended in PBS prior to FACS sorting. The bottom 5% of the IPTG induced culture (low OFF expression) and the top 5% of the IPTG + PPDA (high on expression) were sorted (10 000 events). Following sorting of these two populations, 15 mL of LB + 0.2% glucose was added to the sort tubes. Cells were then pelleted by centrifugation (2500g for 10 min), resuspended in 1 mL of LB + 0.2% glucose, and incubated overnight at 30 °C, 200 rpm. The induction and sorting process was repeated as before, but each population was induced under the alternative condition (IPTG only > IPTG + PPDA, IPTG + PPDA > IPTG only). Sorted cells

were resuspended and concentrated as before and plated onto LB + carbenicillin 100 μg mL^{-1} + 0.2% glucose plates. All FACS analysis was carried out using a Sony SH800. Data were analyzed using FlowJo Single Cell Analysis Software version 10.

Plate-Based Screening Protocol. Single colonies (90 from each FACS sort scheme) were inoculated into 500 μL of LB + carbenicillin 100 μg mL^{-1} + 0.2% glucose and incubated at 37 °C shaking at 1000 rpm for 16 h. This culture was then diluted 100× in LB + carbenicillin 100 μg mL^{-1} + 0.2% glucose in a 96 deep well block prior to incubation for 2 h at 37 °C shaking at 1000 rpm. The culture was then induced with 100 μM of IPTG. Half of the IPTG induced culture was then transferred to another plate and induced with 1000 μM of PPDA. Both plates were incubated for a further 3 h. The resulting culture was harvested by centrifugation at 2250g for 10 min at 4 °C. Cells were then resuspended in 1 mL of PBS and pelleted by centrifugation as before. Finally, cells were again resuspended and diluted 1:1 in PBS. A 200 μL aliquot was then transferred into a black, clear flat-bottomed microplate (Greiner), and the optical density (OD λ = 600 nm) and fluorescence (eGFP fluorescence was measured at λEx/λEm = 488/520 nm, while mKate2 fluorescence was measured at λEx/λEm = 588/633 nm) were recorded. Fluorescence was then normalized to optical density (RFU/OD).

Design of Experiments. The Design of Experiment data structure was generated with JMP 12 pro using the custom design tool. D-optimality was used to select the chosen design from a number of randomly generated designs (random starts = 20 000) to investigate all main effects and two-factor interactions. The factors tested by the D-optimal Design of Experiments are listed in Supplementary Table 4. This design was generated using JMP-12 Pro Custom Design tool based on the D-optimality criteria which scores designs based on reducing the generalized variance around the selected design points, thus giving a more precise estimate of the model effects. The design is a modified fractional factorial design consisting of 40 runs containing 4 center points. The choice of runs was determined by the JMP custom design algorithm. Modeling of the structured experimental data set will allow the prediction of all linear main effects and two-factor interactions. Unlike other fractional factorial DoE designs, the D-optimal custom design allows fractional reduction in the number of experiments required while also facilitating testing of multiple categorical factors (i.e., A or B or C) at more than two levels, making its use essential for DoE testing of the 4 N-terminal linker variants used in this study. An eight-run block was included to control for run order effects and to protect against user error. If human error prevented the use of any data points, this block would mean that only the runs in the respective block need be repeated. Confirmation that this repeated data did not significantly deviate from the rest of the data set is then confirmed when assessing the model effects during SLS regression. SLS model fitting did not assign the block effect as significant. The induction protocol was modified to align with the data structure shown in Supplementary Table 5. Data were collected and processed using the expression conditions described previously. Protein expression was measured after 3 and 24 h. The SLS model fitting and all subsequent experimental expression data (Figure 5D−F) show the eGFP production after 24 h.

Standard Least Squares Model Fitting. Modeling was carried out using the Fit Model function with JMP pro 12. The statistical model was built using the JMP 12 pro Standard Least Squares fit model algorithm using Residual Sum of Squares

(RSS) reduction. Factor importance and factor effects were assessed using ANOVA. The underlying SLS model is represented in this study using the JMP 12 pro Prediction Profiler (Figure 5A and B, Supplementary Figure 6).

Stress Response Promoter Testing: Phosphate Starvation Coupled Riboswitch Function Assay. The P_{phoA}D4-ORS-L35-eGFP and P_{phoA} ΔRS-L35-eGFP constructs were transformed into *E. coli* DH10β TOP10 F′. Single colonies were inoculated into LB containing 100 μg mL^{-1} and incubated for 16 h at 37 °C with shaking at 200 rpm. Cells were then diluted 100× in EZ-rich media and grown to an optical density (λ = 600 nm) of 0.3 (~2.5 h). The culture was centrifuged (2250g, 5 min) and resuspended in an equal volume of EZ-rich media supplemented with either 10, 1.32, 1, 0.1, 0.01, 0.001, or 0.0001 mM K$_2$HPO$_4$. The culture was then aliquoted (500 μL) into a 96-well deep-well block and induced with 0, 40, 200, and 1000 μM PPDA and incubated at 37 °C with shaking at 1000 rpm for 24 h. The OD600 and fluorescence was measured at 24 h. Cells were washed in PBS, and readings were taken as described previously, carried out in biological triplicate.

Expression kinetics of the P_{phoA}::D4-ORS-L35 was also assessed. Cells were treated as above, but following resuspension in K$_2$HPO$_4$ supplemented media, the cell suspension was transferred (1 mL) into a 48 well, baffled deep-well plate (m2p, M2P-48-B) containing either 1000, 400, 200, 40, 8, and 1.6 μM PPDA (P_{phoA}::D4-ORS-L35 only) and incubated in the BioLector culture platform for 24 h at 37 °C with shaking at 1200 rpm. Optical density (λ = 620 nm) and fluorescence (λEx/λEm = 488/520 nm) was measured every 15 min. Carried out in biological triplicate.

Hyperosmotic Shock Activation of P_{osmY} Assay. The P_{osmY}D4-ORS-L35-eGFP and P_{phoA} ΔRS-L35-eGFP constructs were transformed into *E. coli* DH10β TOP10 F′. Single colonies were inoculated into LB containing 100 μg mL^{-1} and incubated for 16 h at 37 °C with shaking at 200 rpm. Cells were then diluted 100× in LB-rich media and grown to an optical density (λ = 600 nm) of 0.3. The culture was centrifuged (2250 g, 5 min) and resuspended in an equal volume of LB media supplemented with 1, 0.8, 0.6, 0.4, 0.2, or 0.171 M (standard LB) or 0.1 M NaCl. The culture was then aliquoted (500 μL) into a 96-well deep-well block and induced with 0, 40, 200, and 1000 μM PPDA and incubated at 37 °C with shaking at 1000 rpm for 24 h. The OD600 and fluorescence was measured at 3 and 24 h. Cells were washed in PBS, and readings were taken as described previously. This experiment was carried out in biological triplicate.

Hydrogen Peroxide Induction of P_{soxS} Assay. The P_{soxS}D4-ORS-L35-eGFP and P_{soxS} ΔRS-L35-eGFP constructs were transformed into *E. coli* DH10β TOP10 F′. Single colonies were inoculated into LB containing 100 μg mL^{-1} and incubated for 16 h at 37 °C with shaking at 200 rpm. Cells were then diluted 100× in LB-rich media and grown to an optical density (λ = 600 nm) of 0.3. The culture was then aliquoted (500 μL) into a 96-well deep-well block and induced with hydrogen peroxide (0, 0.3, 0.03, 0.003, and 0.0003%) and PPDA (0, 40, 200, and 1000 μM) and incubated at 37 °C with shaking at 1000 rpm for 24 h. The OD600 and fluorescence was measured at 3 and 24 h as previously described. The assay was carried out in biological triplicate.

P_{cstA} Induction Assay. The P_{cstA}D4-ORS-L35-eGFP and P_{cstA} ΔRS-L35-eGFP constructs were transformed into *E. coli* DH10β TOP10 F′. Single colonies were inoculated into LB containing 100 μg mL^{-1} and incubated for 16 h at 37 °C with

shaking at 200 rpm. Cells were then diluted 100× in LB-rich media and grown to an optical density (λ = 600 nm) of 0.3. The culture was centrifuged at 2250g for 5 min. The supernatant was removed, and cells were resuspended in LB media ±5% glucose and aliquoted (500 μL) into a 96-well deep-well block containing PPDA (0, 40, 200, and 1000 μM) and incubated at 37 °C with shaking at 1000 rpm for 24 h. The OD600 and fluorescence was measured at 3 and 24 h as previously described. Samples were measured in biological triplicate.

◼ ASSOCIATED CONTENT

ⓈSupporting Information

The Supporting Information is available free of charge on the ACS Publications website at DOI: 10.1021/acssynbio.9b00017.

> Supplementary Figures, Supporting Information and Methods, and Supplementary Tables 2, 3, 4, 5, 6, and 9 (PDF)

> Supplementary Table 1, all primers, ssDNA, and dsDNA sequences; Supplementary Table 7, SLS model coefficients for each of the predicted responses; Supplementary Table 8, data from BioLector characterization of the P_{phoA}D4-ORS-L35-eGFP device (Figure 9E−H); Supplementary Table 10, information on key plasmid and devices (XLSX)

◼ AUTHOR INFORMATION

Corresponding Author

*E-mail: neil.dixon@manchester.ac.uk.

ORCID ◉

N. Dixon: 0000-0001-9065-6764

Author Contributions

R.K. and N.D. wrote and reviewed the main manuscript text, and R.K. prepared figures. R.K. proposed, designed, planned, and performed the experiments.

Notes

The authors declare no competing financial interest.

◼ REFERENCES

(1) Tamsir, A., Tabor, J. J., and Voigt, C. A. (2011) Robust multicellular computing using genetically encoded NOR gates and chemical 'wires'. *Nature 469*, 212−5.

(2) Wang, B., Kitney, R. I., Joly, N., and Buck, M. (2011) Engineering modular and orthogonal genetic logic gates for robust digital-like synthetic biology. *Nat. Commun. 2*, 508.

(3) Wang, B., and Buck, M. (2012) Customizing cell signaling using engineered genetic logic circuits. *Trends Microbiol. 20*, 376−384.

(4) Li, G.-W., Burkhardt, D., Gross, C., and Weissman, J. S. (2014) Quantifying Absolute Protein Synthesis Rates Reveals Principles Underlying Allocation of Cellular Resources. *Cell 157*, 624−635.

(5) Gorochowski, T. E., Avcilar-Kucukgoze, I., Bovenberg, R. A. L., Roubos, J. A., and Ignatova, Z. (2016) A Minimal Model of Ribosome Allocation Dynamics Captures Trade-offs in Expression between Endogenous and Synthetic Genes. *ACS Synth. Biol. 5*, 710−720.

(6) Borkowski, O., Ceroni, F., Stan, G.-B., and Ellis, T. (2016) Overloaded and stressed: whole-cell considerations for bacterial synthetic biology. *Curr. Opin. Microbiol. 33*, 123−130.

(7) Wittmann, A., and Suess, B. (2011) Selection of tetracycline inducible self-cleaving ribozymes as synthetic devices for gene regulation in yeast. *Mol. BioSyst. 7*, 2419−27.

(8) Win, M. N., and Smolke, C. D. (2007) A modular and extensible RNA-based gene-regulatory platform for engineering cellular function. *Proc. Natl. Acad. Sci. U. S. A. 104*, 14283−8.

(9) Isaacs, F. J., et al. (2004) Engineered riboregulators enable post-transcriptional control of gene expression. *Nat. Biotechnol. 22*, 841−7.

(10) Green, A. A., Silver, P. A., Collins, J. J., and Yin, P. (2014) Toehold Switches: De-Novo-Designed Regulators of Gene Expression. *Cell 159*, 925−939.

(11) Breaker, R. R. (2012) Riboswitches and the RNA world. *Cold Spring Harbor Perspect. Biol. 4*, No. a003566.

(12) Barrick, J. E., and Breaker, R. R. (2007) The distributions, mechanisms, and structures of metabolite-binding riboswitches. *Genome Biol. 8*, R239.

(13) Davis, J. H., Rubin, A. J., and Sauer, R. T. (2011) Design, construction and characterization of a set of insulated bacterial promoters. *Nucleic Acids Res. 39*, 1131−1141.

(14) Farasat, I., et al. (2014) Efficient search, mapping, and optimization of multi-protein genetic systems in diverse bacteria. *Mol. Syst. Biol. 10*, 731.

(15) Ng, C. Y., Farasat, I., Maranas, C. D., and Salis, H. M. (2015) Rational design of a synthetic Entner-Doudoroff pathway for improved and controllable NADPH regeneration. *Metab. Eng. 29*, 86−96.

(16) Rosano, G. L., and Ceccarelli, E. A. (2014) Recombinant protein expression in Escherichia coli: advances and challenges. *Front. Microbiol. 5*, 172.

(17) Regulski, E. E., et al. (2008) A widespread riboswitch candidate that controls bacterial genes involved in molybdenum cofactor and tungsten cofactor metabolism. *Mol. Microbiol. 68*, 918−32.

(18) Watson, P. Y., and Fedor, M. J. (2012) The ydaO motif is an ATP-sensing riboswitch in Bacillus subtilis. *Nat. Chem. Biol. 8*, 963−5.

(19) Ames, T. D., and Breaker, R. R. (2011) Bacterial aptamers that selectively bind glutamine. *RNA Biol. 8*, 82−9.

(20) Lemay, J.-F., et al. (2011) Comparative study between transcriptionally- and translationally-acting adenine riboswitches reveals key differences in riboswitch regulatory mechanisms. *PLoS Genet. 7*, No. e1001278.

(21) Dixon, N., et al. (2010) Reengineering orthogonally selective riboswitches. *Proc. Natl. Acad. Sci. U. S. A. 107*, 2830−5.

(22) Wu, M.-C., et al. (2015) Rational Re-engineering of a Transcriptional Silencing PreQ1 Riboswitch. *J. Am. Chem. Soc. 137*, 9015−21.

(23) Nechooshtan, G., Elgrably-Weiss, M., Sheaffer, A., Westhof, E., and Altuvia, S. (2009) A pH-responsive riboregulator. *Genes Dev. 23*, 2650−2662.

(24) Pham, H. L., et al. (2017) Engineering a riboswitch-based genetic platform for the self-directed evolution of acid-tolerant phenotypes. *Nat. Commun. 8*, 411.

(25) Martini, L., Ellington, A. D., and Mansy, S. S. (2016) An in vitro selection for small molecule induced switching RNA molecules. *Methods 106*, 51.

(26) Weigand, J. E., et al. (2007) Screening for engineered neomycin riboswitches that control translation initiation. *RNA 14*, 89−97.

(27) Desai, S. K., and Gallivan, J. P. (2004) Genetic screens and selections for small molecules based on a synthetic riboswitch that activates protein translation. *J. Am. Chem. Soc. 126*, 13247−54.

(28) Lynch, S. A., Desai, S. K., Sajja, H. K., and Gallivan, J. P. (2007) A high-throughput screen for synthetic riboswitches reveals mechanistic insights into their function. *Chem. Biol. 14*, 173−84.

(29) Wallis, M. G., von Ahsen, U., Schroeder, R., and Famulok, M. (1995) A novel RNA motif for neomycin recognition. *Chem. Biol. 2*, 543−52.

(30) Jenison, R. D., Gill, S. C., Pardi, A., and Polisky, B. (1994) High-resolution molecular discrimination by RNA. *Science 263*, 1425−9.

(31) Yang, J., et al. (2013) Synthetic RNA devices to expedite the evolution of metabolite-producing microbes. *Nat. Commun. 4*, 1413.

(32) Jang, S., et al. (2017) Development of Artificial Riboswitches for Monitoring of Naringenin *In Vivo*. *ACS Synth. Biol. 6*, 2077−2085.

(33) Xiu, Y., et al. (2017) Naringenin-responsive riboswitch-based fluorescent biosensor module for *Escherichia coli* co-cultures. *Biotechnol. Bioeng. 114*, 2235.

(34) Topp, S., et al. (2010) Synthetic riboswitches that induce gene expression in diverse bacterial species. *Appl. Environ. Microbiol. 76*, 7881−4.

(35) Robinson, C. J., et al. (2014) Modular riboswitch toolsets for synthetic genetic control in diverse bacterial species. *J. Am. Chem. Soc. 136*, 10615−24.

(36) Hanson, S., Berthelot, K., Fink, B., McCarthy, J. E. G., and Suess, B. (2003) Tetracycline-aptamer-mediated translational regulation in yeast. *Mol. Microbiol. 49*, 1627−37.

(37) Beilstein, K., Wittmann, A., Grez, M., and Suess, B. (2015) Conditional control of mammalian gene expression by tetracycline-dependent hammerhead ribozymes. *ACS Synth. Biol. 4*, 526−34.

(38) Rieder, R., Lang, K., Graber, D., and Micura, R. (2007) Ligand-induced folding of the adenosine deaminase A-riboswitch and implications on riboswitch translational control. *ChemBioChem 8*, 896−902.

(39) Serganov, A., et al. (2004) Structural Basis for Discriminative Regulation of Gene Expression by Adenine- and Guanine-Sensing mRNAs. *Chem. Biol. 11*, 1729−1741.

(40) Ceres, P., Garst, A. D., Marcano-Velázquez, J. G., and Batey, R. T. (2013) Modularity of select riboswitch expression platforms enables facile engineering of novel genetic regulatory devices. *ACS Synth. Biol. 2*, 463−72.

(41) Ceroni, F., Algar, R., Stan, G.-B., and Ellis, T. (2015) Quantifying cellular capacity identifies gene expression designs with reduced burden. *Nat. Methods 12*, 415−8.

(42) Salis, H. M., Mirsky, E. A., and Voigt, C. A. (2009) Automated design of synthetic ribosome binding sites to control protein expression. *Nat. Biotechnol. 27*, 946−50.

(43) Goodman, D. B., Church, G. M., and Kosuri, S. (2013) Causes and effects of N-terminal codon bias in bacterial genes. *Science 342*, 475−9.

(44) Cambray, G., Guimaraes, J. C., and Arkin, A. P. Evaluation of 244,000 synthetic sequences reveals design principles to optimize translation in Escherichia coli. *Nat. Biotechnol.* (2018). DOI: 10.1038/nbt.4238.

(45) Kudla, G., Murray, A. W., Tollervey, D., and Plotkin, J. B. (2009) Coding-sequence determinants of gene expression in Escherichia coli. *Science 324*, 255−8.

(46) Mutalik, V. K., et al. (2013) Precise and reliable gene expression via standard transcription and translation initiation elements. *Nat. Methods 10*, 354−360.

(47) Cardinale, S., and Arkin, A. P. (2012) Contextualizing context for synthetic biology–identifying causes of failure of synthetic biological systems. *Biotechnol. J. 7*, 856−66.

(48) Kent, R., Halliwell, S., Young, K., Swainston, N., and Dixon, N. (2018) Rationalizing Context-Dependent Performance of Dynamic RNA Regulatory Devices. *ACS Synth. Biol. 7*, 1660−1668.

(49) Folliard, T., et al. (2017) Ribo-attenuators: novel elements for reliable and modular riboswitch engineering. *Sci. Rep. 7*, 4599.

(50) Warhaut, S., et al. (2017) Ligand-modulated folding of the full-length adenine riboswitch probed by NMR and single-molecule FRET spectroscopy. *Nucleic Acids Res. 45*, 5512−5522.

(51) Chen, B., Zuo, X., Wang, Y.-X., and Dayie, T. K. (2012) Multiple conformations of SAM-II riboswitch detected with SAXS and NMR spectroscopy. *Nucleic Acids Res. 40*, 3117−3130.

(52) Dixon, N., et al. (2012) Orthogonal riboswitches for tuneable coexpression in bacteria. *Angew. Chem., Int. Ed. 51*, 3620−4.

(53) Lynch, S. A., and Gallivan, J. P. (2009) A flow cytometry-based screen for synthetic riboswitches. *Nucleic Acids Res. 37*, 184−192.

(54) Davidson, M. E., Harbaugh, S. V., Chushak, Y. G., Stone, M. O., and Kelley-Loughnane, N. (2013) Development of a 2,4-dinitroto-

luene-responsive synthetic riboswitch in E. coli cells. *ACS Chem. Biol. 8*, 234−41.

(55) Page, K., Shaffer, J., Lin, S., Zhang, M., and Liu, J. M. (2018) Engineering Riboswitches *in Vivo* Using Dual Genetic Selection and Fluorescence-Activated Cell Sorting. *ACS Synth. Biol. 7*, 2000.

(56) Fisher, R. A. The Design of Experiments. Edinburgh and London: Oliver & Boyd, 1935.

(57) Ilzarbe, L., Álvarez, M. J., Viles, E., and Tanco, M. (2008) Practical applications of design of experiments in the field of engineering: a bibliographical review. *Qual. Reliab. Eng. Int. 24*, 417−428.

(58) Mandenius, C.-F., and Brundin, A. (2008) Bioprocess optimization using design-of-experiments methodology. *Biotechnol. Prog. 24*, 1191−1203.

(59) Brown, S. R., et al. (2018) Design of Experiments Methodology to Build a Multifactorial Statistical Model Describing the Metabolic Interactions of Alcohol Dehydrogenase Isozymes in the Ethanol Biosynthetic Pathway of the Yeast *Saccharomyces cerevisiae*. *ACS Synth. Biol. 7*, 1676−1684.

(60) Xu, P., Rizzoni, E. A., Sul, S.-Y., and Stephanopoulos, G. (2017) Improving Metabolic Pathway Efficiency by Statistical Model-Based Multivariate Regulatory Metabolic Engineering. *ACS Synth. Biol. 6*, 148.

(61) Guimaraes, J. C., Rocha, M., Arkin, A. P., and Cambray, G. (2014) D-Tailor: automated analysis and design of DNA sequences. *Bioinformatics 30*, 1087−1094.

(62) Liao, J., et al. (2007) Engineering proteinase K using machine learning and synthetic genes. *BMC Biotechnol. 7*, 16.

(63) Govindarajan, S. (2015) Mapping of Amino Acid Substitutions Conferring Herbicide Resistance in Wheat Glutathione Transferase. *ACS Synth. Biol. 4*, 221.

(64) Gustafsson, C., et al. (2012) Engineering genes for predictable protein expression. *Protein Expression Purif. 83*, 37−46.

(65) Muhamadali, H., et al. (2016) Metabolomic analysis of riboswitch containing E. coli recombinant expression system. *Mol. BioSyst. 12*, 350−361.

(66) Shine, J., and Dalgarno, L. (1974) The 3′-terminal sequence of Escherichia coli 16S ribosomal RNA: complementarity to nonsense triplets and ribosome binding sites. *Proc. Natl. Acad. Sci. U. S. A. 71*, 1342−6.

(67) Bonde, M. T., et al. (2016) Predictable tuning of protein expression in bacteria. *Nat. Methods 13*, 233−236.

(68) Espah, B. A., Channarasappa, A. S., and Salis, H. M. (2014) Translation rate is controlled by coupled trade-offs between site accessibility, selective RNA unfolding and sliding at upstream standby sites. *Nucleic Acids Res. 42*, 2646−2659.

(69) Torgerson, C. D., Hiller, D. A., Stav, S., and Strobel, S. A. (2018) Gene regulation by a glycine riboswitch singlet uses a finely tuned energetic landscape for helical switching. *RNA 24*, 1813.

(70) Lorenz, R., et al. (2011) ViennaRNA Package 2.0. *Algorithms Mol. Biol. 6*, 26.

(71) Marshak, A. (1951) The purine and pyrimidine content of three strains of Escherichia coli. *Science 113*, 181−2.

(72) Registry of Standard Biological Parts. http://parts.igem.org/Promoters/Catalog/Anderson, accessed January 17, 2018.

(73) Ceroni, F. (2018) Burden-driven feedback control of gene expression. *Nat. Methods 15*, 387.

(74) Dahl, R. H., et al. (2013) Engineering dynamic pathway regulation using stress-response promoters. *Nat. Biotechnol. 31*, 1039−1046.

(75) Song, H., Jiang, J., Wang, X., and Zhang, J. (2017) High purity recombinant human growth hormone (rhGH) expression in Escherichia coli under phoA promoter. *Bioengineered 8*, 147−153.

(76) Yim, H. H., and Villarejo, M. (1992) osmY, a new hyperosmotically inducible gene, encodes a periplasmic protein in Escherichia coli. *J. Bacteriol. 174*, 3637−44.

(77) Yim, H. H., Brems, R. L., and Villarejo, M. (1994) Molecular characterization of the promoter of osmY, an rpoS-dependent gene. *J. Bacteriol. 176*, 100−7.

(78) Weichart, D., Lange, R., Henneberg, N., and Hengge-Aronis, R. (1993) Identification and characterization of stationary phase-inducible genes in Escherichia coli. *Mol. Microbiol. 10*, 407−20.

(79) Krapp, A. R., Humbert, M. V., Stor, N., Correspondence, C., and Carrillo, N. S. (2018) The soxRS response of Escherichia coli can be induced in the absence of oxidative stress and oxygen by modulation of NADPH content. *Microbiology*, 1633.

(80) Carlson, P. D., and Lucks, J. B. (2019) Elements of RNA Design. *Biochemistry 58*, 1457.

(81) Blommel, P. G., Becker, K. J., Duvnjak, P., and Fox, B. G. (2007) Enhanced bacterial protein expression during auto-induction obtained by alteration of lac repressor dosage and medium composition. *Biotechnol. Prog. 23*, 585−98.

(82) Chae, Y. K., Cho, K. S., Chun, W., and Lee, K. (2003) Protein production by stationary phase induction (SPI). *Protein Pept. Lett. 10*, 369−74.

(83) Dahl, R. H., et al. (2013) Engineering dynamic pathway regulation using stress-response promoters. *Nat. Biotechnol. 31*, 1039−1046.

(84) Horga, L. G., et al. (2018) Tuning recombinant protein expression to match secretion capacity. *Microb. Cell Fact. 17*, 199.

(85) Hanahan, D. *DNA Cloning Techniques: A Pratical Approach*; IRL Press, 1985.

(86) Neidhardt, F. C., Bloch, P. L., and Smith, D. F. (1974) Culture medium for enterobacteria. *J. Bacteriol. 119*, 736−47.

(87) Carr, S. B., Beal, J., and Densmore, D. M. (2017) Reducing DNA context dependence in bacterial promoters. *PLoS One 12*, No. e0176013.